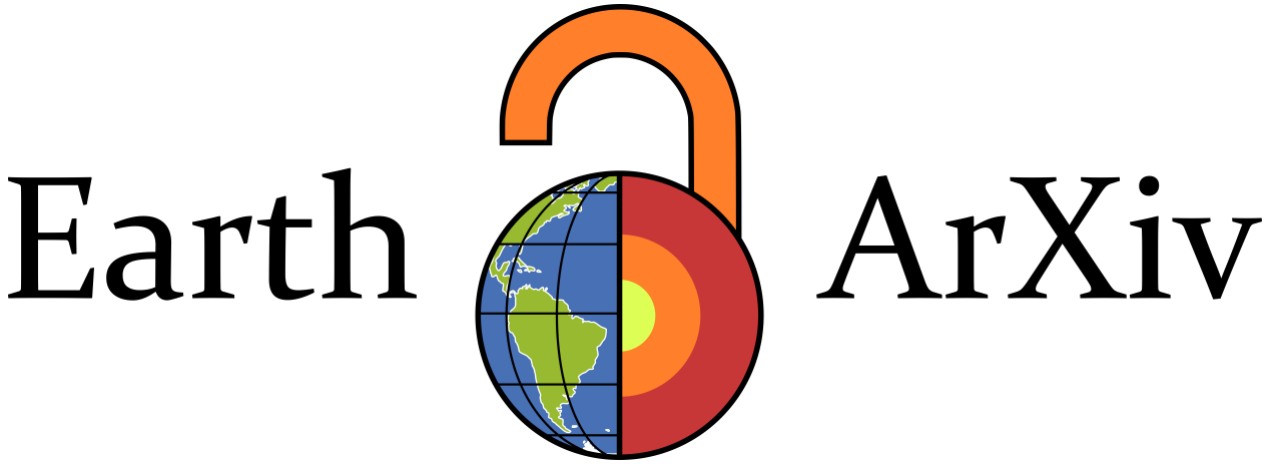

Investigating the Formation Conditions of Evaporitic Chloride, Carbonate, and Sulfate Paragenetic Assemblages on Early Mars

Eashan Das[1], Kaushik Mitra[1,2,3†], Joel A. Hurowitz[1], Timothy D. Glotch[1], and Yatharth Bahl[1]

[1]Department of Geosciences, Stony Brook University, Stony Brook, NY 11794 USA.

[2]Department of Earth & Planetary Sciences, The University of Texas at San Antonio, San Antonio, TX 78249 USA

[3]Department of Physics & Astronomy, The University of Texas at San Antonio, San Antonio, TX 78249 USA.

†Corresponding author:

Kaushik Mitra (kaushik.mitra@utsa.edu)

Investigating the Formation Conditions of Evaporitic Chloride, Carbonate, and Sulfate Paragenetic Assemblages on Early Mars

Eashan Das[1], Kaushik Mitra[1,2,3]†, Joel A. Hurowitz[1], Timothy D. Glotch[1], and Yatharth Bahl[1]

[1]Department of Geosciences, Stony Brook University, Stony Brook, NY 11794 USA.

[2]Department of Earth & Planetary Sciences, The University of Texas at San Antonio, San Antonio, TX 78249 USA

[3]Department of Physics & Astronomy, The University of Texas at San Antonio, San Antonio, TX 78249 USA.

†Corresponding author:

Kaushik Mitra (kaushik.mitra@utsa.edu)

Keywords: Evaporite; Chloride; Carbonate; Sulfate; Mars

Abstract:

Aqueous alteration minerals, such as chlorides, carbonates, and sulfates, have been discovered on the surface of Mars by both orbital and in situ rover observations. Alteration minerals require liquid water for their formation and can place critical constraints on the geochemistry of the aqueous systems in which they are formed. Primary mineralization facilitated by evaporation of weathering fluids is an important mineral formation pathway that can produce alteration minerals, such as chlorides, carbonates, and sulfates on Mars. Here, we simulate basalt weathering under diverse Mars-relevant conditions and study the chemical composition of the resultant fluid 'leachates.' We categorize and group ~60 different leachates on the basis of relative concentrations of major cations (Na^{+}, Mg^{2+}, Ca^{2+}, Fe^{2+}) and anions (Cl^{-}, SO_4^{2-}, HCO_3^{-}) and predict 8 major leachate types possible on early Mars. We simulated the evaporation of all leachates and studied the consequent precipitation of evaporite minerals. Our results indicate that sulfate-rich leachates were the most prevalent, which upon evaporation generated a variety of Mg/Ca/Fe sulfates. Siderite ($FeCO_3$) precipitated during closed system weathering of basalt under relatively low volcanic activity on Mars. The results of our study can explain the widespread presence of sulfate salts and the recent detection of siderite in the sulfate-rich Mirador formation at Gale crater. Halite (NaCl) was the major chloride mineral that precipitated in our models and was exclusively produced in closed system, water-limited, and high initial acidity conditions.

1. Introduction

Compared to Earth, Mars today is a dry planet. However, there is ample evidence of substantial liquid water activity on the surface of early Mars (Craddock & Howard, 2005; Irwin et al., 2005a; 2005b; Ramirez & Craddock, 2017). Mineralogical evidence of past liquid water activity includes the presence of aqueous alteration minerals, henceforth 'alteration minerals', detected on the surface of Mars by both orbital and in situ rover investigations (Bibring et al., 2006; Murchie et al., 2009; Ehlmann & Edwards, 2014; Buz et al., 2017; Sun et al., 2023; Royer et al., 2025). Their global distribution suggests that a substantial portion of Mars' past water budget is likely sequestered within these alteration minerals (Ehlmann & Edwards, 2014; Scheller et al., 2021). Understanding the formation processes of these minerals can provide valuable insight into the past geochemical environments on early Mars.

Alteration minerals can form via both primary and secondary mineralization pathways. Primary mineralization is the direct crystallization of a mineral from a fluid phase (Hazen et al., 2023), for example in hydrothermal vents, hot springs, geysers, hydrothermal veins/fractures, and chemical precipitation. On the other hand, minerals may form by secondary mineralization through the chemical weathering or alteration (henceforth referred to simply as weathering) of pre-existing minerals through fluid-rock interaction. The fluids produced due to weathering (also referred to as 'leaching') are called leachates and can produce salts upon their evaporation or freezing (Hazen et al., 2023; Marion and Kargel, 2008; Elsenousy et al., 2015). Evaporite minerals represent the final stages of liquid water availability in a geological setting. They are characteristic of the evaporating leachate and can, therefore, place critical constraints on the geochemical conditions of their formation (e.g., Eugster & Hardie, 1978; Lowenstein & Hardie, 1985; Tosca et al., 2005; Tosca & McLennan, 2006; Toner et al., 2015). Common evaporite minerals found on Mars include sulfates, carbonates, and chlorides (Osterloo et al., 2008; Murchie et al., 2009; Ehlmann & Edwards, 2014; Hazen et al., 2023). Hundreds of sulfate, chloride, and carbonate detections have been made using both orbital and *in situ* measurements (Bibring et al., 2006; Murchie et al., 2009; Ehlmann & Edwards, 2014; Osterloo et al., 2008; 2010; Glotch et al., 2010; Niles et al., 2012; Wray et al. 2016), many of which may be evaporative in origin (Tosca et al., 2005; Tosca & McLennan, 2006).

While evaporite deposits on Earth typically exhibit a progression from carbonates to sulfates and finally to chlorides (Hardie, 1968; Eugster & Hardie, 1978; Jones & Decampo, 2003), alteration assemblages containing chloride-sulfate-carbonate salts together at the same location is

rare on Mars (Ehlmann & Edwards, 2014; Leask et al., 2024). Specifically, chloride-bearing deposits are not observed in association with other evaporite minerals that are usually found in terrestrial environments (Osterloo et al., 2008; 2010; Glotch et al., 2010; Ye & Glotch, 2019; Leask & Ehlmann, 2022). Widespread across the southern highlands, chloride deposits are typically isolated from carbonate and sulfate salts but occasionally occur alongside, but stratigraphically above, ancient phyllosilicate-bearing strata (Osterloo et al., 2008; 2010; Murchie et al., 2009; Glotch et al., 2010; 2016, Ye & Glotch, 2019; Leask & Ehlmann, 2022; Leask et al., 2024). Chloride salts may precipitate under a wide range of pH conditions, unlike carbonates or sulfates that are often favored under alkaline and acid conditions, respectively (Tosca & McLennan, 2006).

While chloride salts on Mars are likely to be exclusively evaporitic (Tosca & McLennan, 2006), carbonate and sulfate salts could be produced by both evaporative and non-evaporative pathways (Hazen et al., 2023). Additionally, Fe/Mg carbonate deposits on Mars are more localized and occasionally co-occur with sulfate minerals (Ehlmann et al., 2008; Wray et al., 2016; Bridges et al., 2019; Horgan et al., 2020; Zastrow et al., 2021; Clave et al., 2023; Clark et al., 2024; Tutolo et al., 2025). Because carbonate precipitation is typically favored under alkaline conditions, its association with sulfates, suggests a complex interplay between primary and secondary mineralization pathways (Fairen et al., 2004; Niles et al., 2013; Kite et al., 2025; Tutolo et al., 2025). While Ca/Mg sulfates do not necessitate acidic conditions of formation, the presence of Al/Fe sulfates indicate weathering under an acidic environment, which was either derived volcanically or by the alteration of sulfide minerals. Sulfate salts also remain spatially isolated from known chloride deposits on Mars (Squyres et al., 2004; Gendrin et al., 2005; Langevin et al., 2005; Bibring et al., 2006; King & McLennan, 2010; Murchie et al., 2009; Buz et al., 2017). The reasons for the general isolation of chloride-carbonate-sulfate deposits are not well known and indicates a poorly constrained understanding of evaporite mineral formation on Mars. Therefore, a thorough examination of the paragenetic relationship among key evaporite minerals (i.e., sulfates, chlorides, and carbonates) is essential to understand aqueous systems on early Mars.

Simulating weathering and leachate evolution under a volcanically active Mars could provide unique insights into how various conditions may have shaped leachate chemistry, offering key perspectives into the origins of Martian evaporite deposits. We simulated martian basalt weathering under a wide array of volcanic and hydrologic conditions on early Mars to assess how various physicochemical factors (e.g., water-to-rock ratio, amounts of volcanically derived

volatiles) influenced leachates generated from it. We studied the composition of the leachates and grouped them into different compositional types based on the concentration of cations, anions, and pH. We also simulated the evaporation of leachates and studied the resulting evaporite mineral assemblages. Using results from a wide variety of alteration conditions, we discuss scenarios that can explain primary mineralization of chloride, carbonate, and sulfate salts from evaporation of martian brines.

2. Methods

Using thermodynamic modeling, we simulated the chemical weathering of basalt under atmospheric and geochemical conditions representative of volcanically active and quiescent periods on early Mars. In a prior study, we simulated basalt weathering under a diverse set of conditions plausible on early Mars and investigated paragenetic alteration mineral assemblages (Das et al., 2026). While the earlier study investigated the mineral products of basalt alteration, this study focuses on chemistry of the resulting weathering fluid (aka leachate) and the mineral products formed upon their evaporation. Here, we analyzed all fluids produced at the end of the alteration (i.e., leachates), identified and characterized characteristic fluid types based on their composition, and proposed different leachate types possible as a result of basalt alteration on early Mars. We then modeled evaporation of leachates and investigated the minerals produced as a result.

We simulated the weathering of the '*Mazatzal*' basalt, taken to represent the average Martian crust (McSween 2004; 2006a; 2006b; 2008; 2009; 2015) (Table S1), at 25ºC under a fixed pO_2 (0.05 bar). Owing to the availability of the most extensive thermodynamic dataset, we simulated rock weathering on the surface of Mars at 298 K (25°C). We fix pO_2 values to 0.05 bar, which is most likely close to the maximum possible available in the Martian atmosphere throughout its history (Wordsworth et al., 2021; Mitra et al., 2023). The amount of carbon dioxide (CO_2) gas in the early atmosphere of Mars likely varied over time, possibly between 0.05 and 1 bar (Wordsworth et al., 2021). The amount of S-gases degassed over time by volcanism (e.g., SO_2, H_2S) (Bellino and Sun, 2025) and the resulting acidity is incorporated into the geochemical models by assuming an initial sulfuric acid acidity [H_2SO_4] equal to 10^{-3}, 0.5 and 1 moles per liter. We constrained the amount of Cl in our geochemical system by assuming a hypothesized global S to Cl ratio of 3.7 (Ojha et al., 2018). The variation in the amount of water available on Mars was

accounted for by allowing a fixed amount of the basalt to interact with different ratios of water: W/R varied from 0.1 to 10^6. To summarize, we conducted 60 different geochemical models to investigate Mazatzal basalt weathering at 25°C under 0.05 bar O_2, in two different pCO_2 conditions (0.05 and 1 bar), three different concentrations of H_2SO_4 [10^{-3}, 0.5, and 1 mol L^{-1}], a fixed S/Cl ratio (3.7), at five different water-to-rock (W/R) ratios [10^{-1}, 1, 10, 10^3, and 10^6] under both open 'buffered' and closed 'unbuffered' system conditions (Figure 1). Our model parameter workspace emulates and extends that used in earlier studies in order to compare and contrast the mineral products of alteration (Catalano, 2013; Das et al., 2026; Zolotov and Mironenko, 2007) with the leachates and subsequently the minerals produced by their evaporation.

159

160

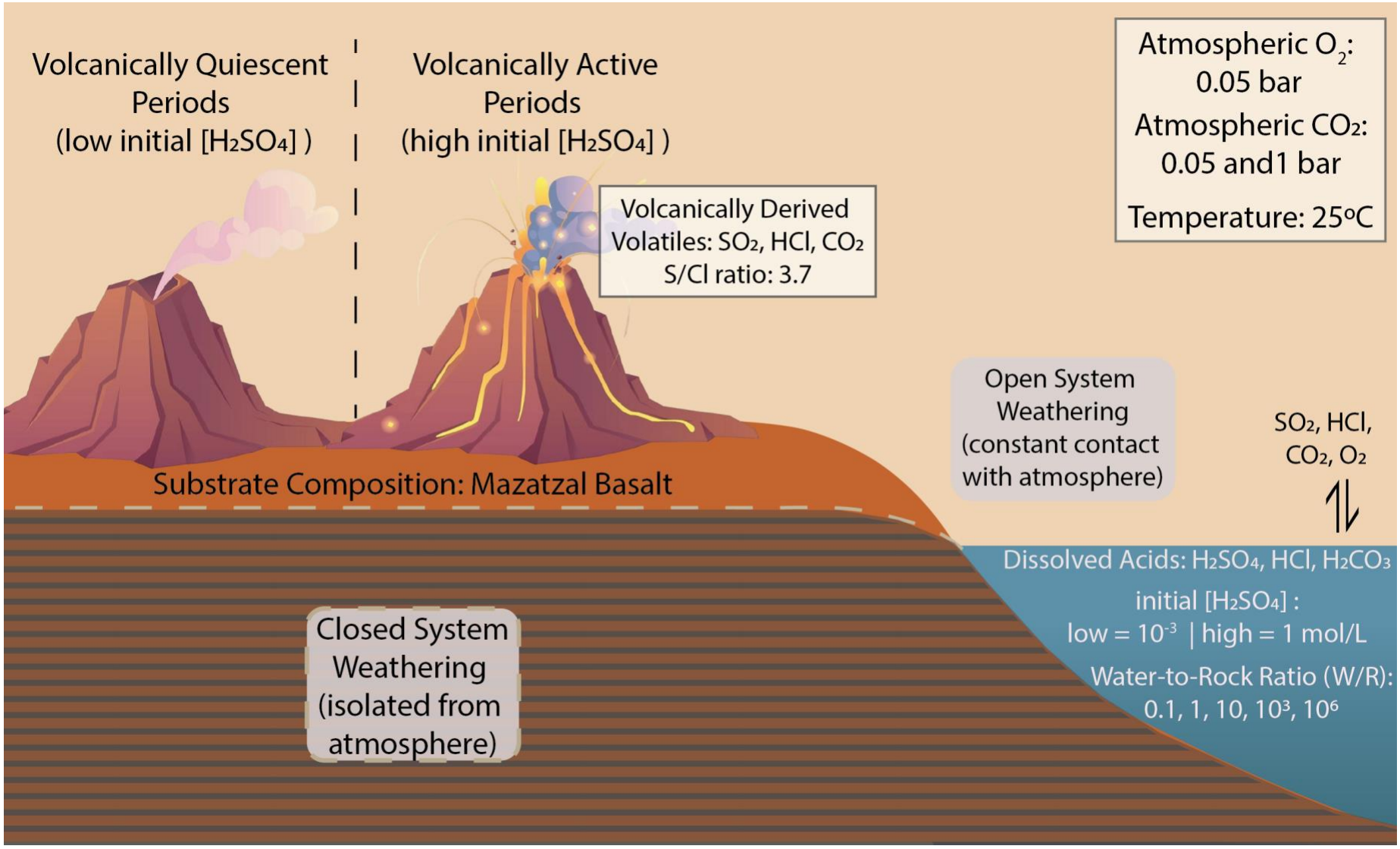

161

162 *Figure 1: Schematic diagram illustrating various model workspace parameters chosen in our modeling study*

2.1 Model Setup and Database

We undertake a thermodynamic modeling approach that predicts the mineral and fluid products of weathering and the subsequent evaporation of alteration fluids using a Gibbs free energy minimization algorithm. We used the *React* module of the Geochemist's Workbench (GWB) software (Bethke, 2022) to model basalt alteration under different Mars-relevant geochemical conditions. We used an updated version of the thermodynamic database produced by the Lawrence Livermore National Laboratory, V8-R6+ (Catalano, 2013; Delany and Lundeen, 1991). We added thermodynamic data for chlorapatite [$Ca_5(PO_4)_3Cl$] as it is an important Cl-bearing phase in Martian basalts and therefore an important source of chlorine in Martian aqueous systems (Blanc et al., 2012). While the rates of mineral dissolution and alteration play a vital role in determining the fate of minerals during alteration, we limit our study to thermodynamic modeling only, owing to the lack of kinetic data of several mineral phases pertinent to our reaction conditions. However, we suppressed those minerals that are unlikely to form in the pressure-temperature conditions relevant to the geochemical system owing to sluggish kinetics (see supplementary section S1 for full list of suppressed phases).

2.2 Types of Geochemical Models

2.2.1 Leaching Models

We initiated *React* models by providing the weight percentages of the individual minerals that comprise the *Mazatzal* basalt (Table S1), the alteration fluid relative to the rock, and the composition of the atmosphere that we assume to be in equilibrium with the leaching system. The system is then allowed to react and predict, thermodynamically, the most stable fluid assemblage possible when the fluid interacts with the substrate. Concentrations of cations (especially H^+, Fe^{2+}, Ca^{2+}, Mg^{2+}, Na^+) and anions (especially Cl^-, SO_4^{2-}, CO_3^{2-}) were tracked in the resulting solution (data in Zenodo repository Das & Mitra, 2026).

2.2.2 Classification of Leachates

The leachate solutions not only hold information about the alteration process but also produce minerals upon their evaporation (or freezing). While our simulations produced 60 different leachates, upon close examination, we observed similarities in the solution composition. Based upon the similarities in their compositions, we grouped the resulting fluids into different

194 'leachate types' using the k-means statistical clustering algorithm (see supplementary section S2
195 for details). Using a combination of statistical clustering and geochemical ternary diagrams
196 (Supplementary Figures S1-S2), we grouped and classified all 60 leachate solutions into distinct
197 leachate types on the basis of their ionic compositions and pH.
198
199 *2.2.3 Evaporation of Leachates*
200 We simulated the evaporation of leachates and studied their evolution and the consequent
201 formation of evaporite minerals by simulating evaporation in *React* using the FREZCHEM
202 database (Marion et al., 2010). The FREZCHEM database uses Pitzer ion interaction model
203 (Pitzer, 1973; 1991, Harvie et al., 1984; Drever, 1997) designed for high ionic strength solutions
204 and has been used in several studies simulating evaporation and/or freezing on Mars (e.g., Marion
205 et al., 2008; Marion et al., 2013; Elsenousy et al., 2015; Catling et al., 2015). However, theoretical
206 evaporation models can fail to converge in extreme cases resulting in partial assessment of
207 evaporite assemblage. In such cases, we estimate mineral assemblages by analyzing the
208 composition of leachate using principles of chemical divides and drawing on results from
209 terrestrial leachate evolution studies (Hardie & Eugster, 1970; Eugster & Hardie, 1978; Tosca &
210 McLennan, 2006).
211
212 **3. Results**
213 ***3.1 Leaching Models***
214 Leachates produced by the chemical alteration of a rock are primarily controlled by the
215 composition of the substrate, the alteration fluid, and the environmental conditions encountered
216 during weathering. While basalt serves as the source of metals (Fe, Mg, Na, Ca, Si) in both the
217 leachate and the alteration mineral assemblage, the anions are primarily sourced by the alteration
218 fluid. The volcanic outgassing of CO_2, S-containing gases (H_2S, SF_6, or their oxidized products
219 such as SO_2/SO_3), and HCl is the primary source of anions (e.g., bicarbonate (HCO_3^-), carbonate
220 (CO_3^{2-}), sulfate (SO_4^{2-}), and chloride (Cl^-)) in the alteration fluid.
221 The identity and concentration of the anions in the leachate is determined by the oxidation
222 state of the non-metal and the fluid pH. Chlorine is the simplest major non-metal in our study since
223 it exists solely as Cl^-. Carbon, on the other hand, can exhibit a wide range of oxidation states from
224 -4 in most organic molecules, such as methane (CH_4), to +4 in inorganic compounds such as CO_2,

carbonic acid (H_2CO_3), carbonates (CO_3^{2-}), and bicarbonate (HCO_3^-). The conversion of inorganic carbon to organic compounds was prohibited in our models as those conversions usually need elevated temperatures and pressures or biological intervention and therefore not relevant to our modeling conditions. The dissolved inorganic carbon (DIC) in the leachates is oxidized [C(IV)] and speciate as a function of pH: carbonic acid [H_2CO_3] at pH < 6.35; bicarbonate [HCO_3^-] between pH 6.35 and 10.35; carbonate [CO_3^{2-}] at pH > 10.35. Sulfur exhibits slightly more complicated oxidation states and pH dependence. Sulfur mostly existed in its oxidized state [S(VI)], either as bisulfate (HSO_4^-) below pH 2 or as sulfate above pH 2. However, at highly alkaline pH (~12), sulfur experienced a reduction in its oxidation state and existed as sulfide (HS^-). Here, we present the concentration of individual ions (e.g., Fe(II)) as the sum of all complexed species (e.g., Fe(II)(aq.), $FeCl^+$, $FeCl_2$(aq.), $FeSO_4$(aq.)) present in the leachate. While we only discuss results that are focused on the boundary condition values of initial sulfuric acid concentrations [10^{-3} and 1 mol L^{-1}], to underscore the effect of initial system acidity, leachate compositions at all initial sulfuric acid concentrations are presented in the supplementary information (Figures S3-S4).

3.1.1 Fluid Chemistry of Leachates

The fluid chemistry of leachates was primarily determined by the system openness and initial sulfuric acid [H_2SO_4] concentration of the alteration fluid. The amount of water relative to the rock undergoing alteration influenced the fluid concentration, especially the cations. While pCO_2 determined the initial amount of DIC in the solution, its effect on the concentrations of other ions in the leachate are less pronounced than sulfuric acid content and W/R.

Leachates produced in open system were predominated by S(VI), particularly at high initial [H_2SO_4] (Figure1 a to d; Table 1); S(VI) speciated as SO_4^{2-} at pH >2, while HSO_4^- dominated in leachates with pH below ~2. The concentration of S(VI) decreases with increasing W/R in systems starting with low but remains constant at high initial [H_2SO_4]. C(IV) typically predominated over other anions when basalt underwent weathering by a large amount of fluid under low initial acidity. Cl- concentration remained lower than S(VI) in all leachates produced in open system but was higher than C(IV) in highly acidic alteration fluids. While an increased W/R decreased Cl- concentration in low acidic fluids, it had an imperceptible effect when alteration fluid was highly acidic. The major cation in open systems was Mg^{2+}; Na^+ and Ca^{2+} followed Mg^{2+} concentration

closely, particularly at higher W/R (Figure 2 e to h). Fe^{2+} was depleted at low initial [H_2SO_4] but increased noticeably at high initial [H_2SO_4]; concentration of Fe^{3+} always remained negligible compared to Fe^{2+}. All cations reached similar concentrations at W/R > 10^3. Concentration of all ions showed a decreasing trend with increasing W/R, except Fe^{2+} at low initial [H_2SO_4], where it maintained its low concentration.

In contrast, closed system leachates showed greater compositional variability (Figure 2 i to 2l). At low initial [H_2SO_4], C(IV) predominated across all W/R and both pCO_2 conditions, except at W/R = 10, where its concentrations was lowest among the major anions, thereby reversing the relative concentration trend (Figure 2i and 2k). Although dilute, S likely speciated as HS^- in this high alkaline solution with Cl^-. At low initial [H_2SO_4], concentration of total dissolved sulfur remained low and relatively constant; increasing W/R (> 10^3) decreased the final pH of these leachates between 8 and 2 that stabilized SO_4^{2-}. However, at high initial [H_2SO_4], S(VI) concentration resembled a step function when W/R increased from 1 to 10. Chloride concentration was highest at low W/R (<10) while S(VI) dominated at higher W/R. While pCO_2 did not exert a major control on Cl- and S(VI), C(IV) concentration increased with increasing CO_2 in the atmosphere. C(IV) concentration in high initial acidity fluids also demonstrated a step-wise trend from W/R 1 to 10. While increasing with greater amount of highly acidic alteration fluid, C(IV) concentration remained lower than S(VI) and Cl^-.

Cation chemistry in closed systems was markedly different in closed weathering systems as compared to open systems (Figure 2m to 2p). Concentration of Na^+ predominated all closed system leachates at low W/R (~1 to 10) but decreased and became equivalent to other cations concentration at higher W/R (>10^3). Mg^{2+} concentrations were substantially lower in closed systems as compared to open systems. At low initial [H_2SO_4], [Mg^{2+}] was negligible at W/R <10 but surged at W/R = 10^3. At high initial [H_2SO_4], a similar trend was observed, and Mg^{2+} concentration peaked at W/R~10. Ca^{2+} concentration was influenced by W/R and initial [H_2SO_4] but not pCO_2. [Ca^{2+}] showed a slow increasing trend under low initial [H_2SO_4] conditions until W/R = 10^3. Under high initial [H_2SO_4] conditions, greater [Ca^{2+}] were observed, and showed trends similar to Na^+.

Ferrous iron (Fe^{2+}) displayed the most complicated trends. It was dependent on initial [H_2SO_4], W/R, and pCO_2. Fe^{2+} concentration decreased with increase in W/R at low [H_2SO_4] and low pCO_2. When pCO_2 was increased to 1 bar, [Fe^{2+}] at each W/R remained similar to their

corresponding low pCO_2 counterparts, except at W/R=10 that showed a 10^4-fold increase. Increasing the initial [H_2SO_4] had a drastic effect on [Fe^{2+}]. At high [H_2SO_4], [Fe^{2+}] was lower than its low initial [H_2SO_4] counterparts at low W/Rs (0.1 and 1); at W/R=10, Fe^{2+} concentration rapidly increased relative to low initial [H_2SO_4]. However, at W/R$\geq 10^3$ [Fe^{2+}] was the same at low and high initial [H_2SO_4]. pCO_2 had no effect on the Fe^{2+} concentration at high initial [H_2SO_4].

3.1.2 Partitioning of Elements between Fluid and Mineral Phases

In open systems, partitioning of elements between solution and minerals systematically varied with W/R and initial [H_2SO_4]; pCO_2 did not have an observable effect on cation partitioning in the open system (Figures 3 and 4). Cl^- and C(IV) partitioned entirely in the solution in open systems across all conditions. S(VI) was dominantly mineral bound forming Ca/Al/Fe sulfates at W/R $\leq$10 and low initial [H_2SO_4] but dissolved when either initial acidity or W/R increased. Mg^{2+} and Na^+ were entirely soluble across modeled conditions. Fe^{2+} was dominantly mineral bound at low initial [H_2SO_4]. At high initial [H_2SO_4], Fe^{2+} was primarily mineral bound at low W/R, becoming entirely solution bound as W/R was increased. Ca^{2+} was mostly mineral bound at low and medium W/R and was solution bound at high W/R, regardless of initial [H_2SO_4].

In the closed system, Cl^- partitioned in the solution, while C(IV) demonstrated affinity to the mineral phase under medium to low W/R. When [H_2SO_4] was low, C(IV) remained dissolved at low and high W/R, except at W/R = 10, under which carbonates were produced. At high initial [H_2SO_4], C(IV) was dominantly mineral bound at low W/R but completely dissolved at W/R $\geq$ 10. S(VI) exhibited the greatest variability in relative partitioning between solution and mineral. At low initial [H_2SO_4], S(VI) formed sulfates at high pCO_2 and medium W/R [~10]; at high initial [H_2SO_4], sulfate minerals were formed only at low W/R ratio and became increasingly soluble as W/R increased; pCO_2 had no effect on S(VI) solubility under high [H_2SO_4] acidity.

In the closed system, Na^+ was predominantly mineral bound at low W/R (~0.1) at both low and high initial [H_2SO_4]. Mg^{2+} was dominantly mineral bound at low and medium W/R but became soluble at high W/R and low initial [H_2SO_4]; at high initial [H_2SO_4], Mg^{2+} was mineral bound at low W/R but then became soluble at W/R $\geq$10. Fe^{2+} was primarily mineral bound at low initial [H_2SO_4]; at high initial [H_2SO_4], Fe^{2+} was dominantly mineral bound at low W/R (~0.1), then solubilized as W/R increased. Ca^{2+} was primarily mineral bound at low and medium W/R and

entirely dissolved at high W/R at both low and high initial [H_2SO_4]. A slight increase in Ca^{2+} solubility was observed at W/R ~10 at high pCO_2.

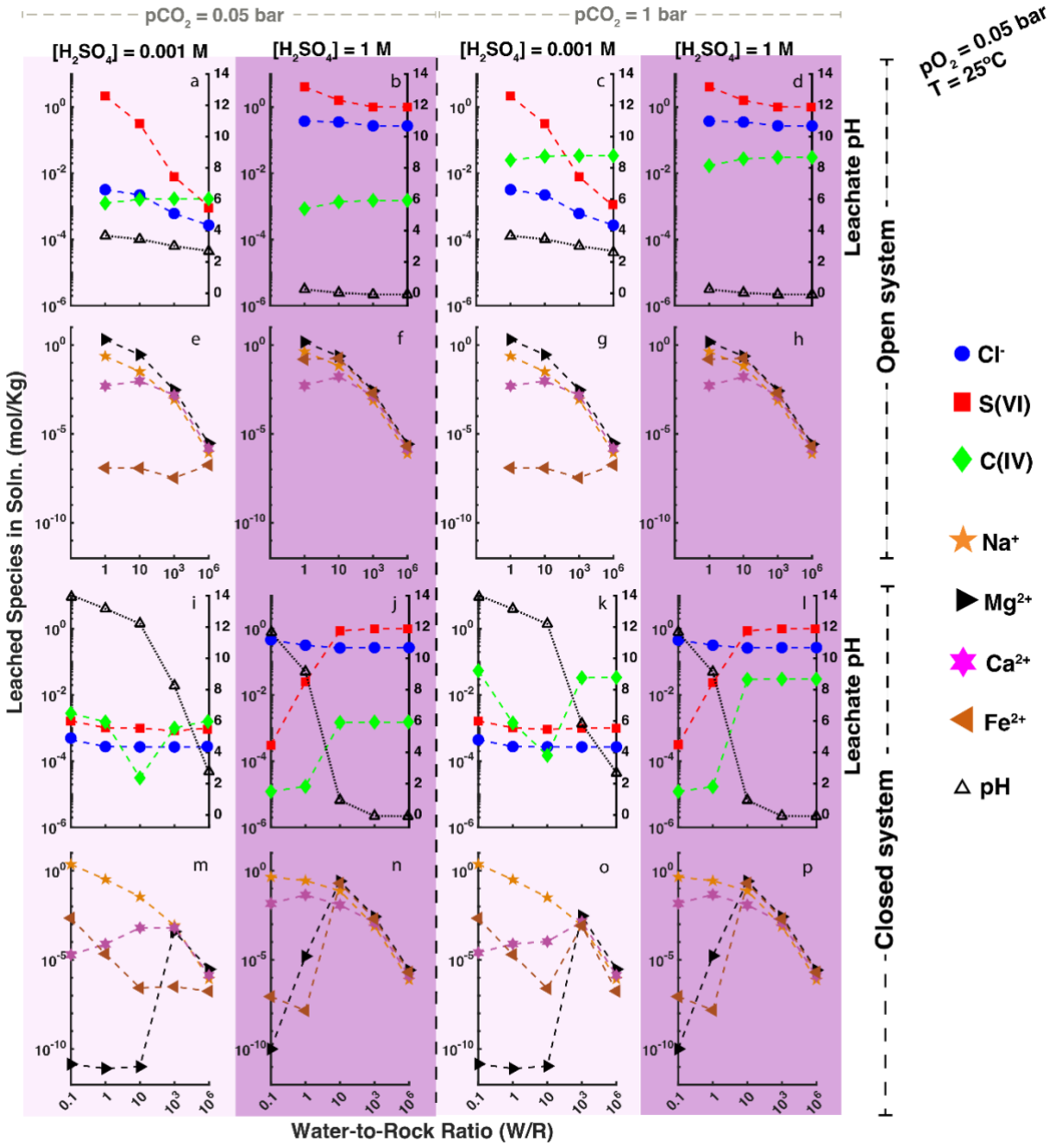

***Figure 2**: Concentrations of major species in leachate solutions (in mol/Kg) generated from our models. Here we show quantities of major evaporite mineral forming anions in the leachate (Cl^-, C(IV), S(VI)) and cations (Na^+, Mg^{2+}, Fe^{2+}, Ca^{2+}) as Water-to-Rock ratio (W/R) is varied from 0.1 to 10^6, at low initial [H_2SO_4] = 0.001 mol L^{-1} and pCO_2 = 0.05 bar (light purple - a,e, i,m; c,g,k,o) and high initial [H_2SO_4] = 1 mol L^{-1} and pCO_2 = 1 bar (dark purple - b,f,j,n; d,h,l,p). Open system modeling results are shown in a) through h), while closed system results are shown in i) through p). Note models did not successfully run for W/R = 0.1 for open system models, so results are shown for W/R = 1 to 10^6. pH of the generated leachates is indicated by open triangles and dashed lines on the right axis of the graphs that display leached anion quantities (a-d; i-l). While sulfur exists as S(VI) [either sulfate or bisulfate] in most fluids, it exists as sulfide under highly alkaline conditions.*

331 ***Table 1:*** *General trends of anion and cation concentration and the major minerals precipitated during the simulated chemical*
332 *weathering of Mazatzal basalt as a function of system openness, initial [H_2SO_4], pCO_2, and W/R.*

Initial [H_2SO_4] (mol L^{-1})	**pCO_2 (bar)**	**Anion Distribution**	**Cation Distribution**	**Major Alteration Minerals Formed**
Open System				
10^{-3}	0.05	W/R 1-10: S(VI) >> Cl^- ≥ C(IV) W/R 10^3: S(VI) > C(IV)> Cl^- W/R 10^6: C(IV)≥ S(VI)> Cl^-	W/R 1-10: $Mg^{2+} > Na^+ > Ca^{2+} >> Fe^{2+}$ W/R 10^3: $Mg^{2+} \geq Na^+ \geq Ca^{2+} >> Fe^{2+}$ W/R 10^6: $Mg^{2+} \geq Na^+ \geq Ca^{2+} \geq Fe^{2+}$	W/R 1-10: Fe/Mg smectites, Ca/Al sulfates, Al sulfates, Zeolites W/R 10^3: Fe/Mg smectites, Zeolites W/R 10^6: Oxides
1	0.05	S(VI) > Cl^- >> C(IV)	W/R 1-10: $Mg^{2+} > Na^+ > Fe^{2+} > Ca^{2+}$ W/R 10^3-10^6: $Mg^{2+} \geq Na^+ \geq Fe^{2+} \geq Ca^{2+}$	W/R 1: Zeolites, Fe sulfates, Ca sulfates W/R 10: Zeolites, Ca sulfates W/R 10^3: Zeolites W/R 10^6: No Minerals
10^{-3}	1	W/R 1-10: S(VI) >> C(IV) > Cl^- W/R 10^3-10^6: C(IV)> S(VI)> Cl^-	W/R 1-10: $Mg^{2+} > Na^+ > Ca^{2+} >> Fe^{2+}$ W/R 10^3: $Mg^{2+} \geq Na^+ \geq Ca^{2+} >> Fe^{2+}$ W/R 10^6: $Mg^{2+} \geq Na^+ \geq Ca^{2+} \geq Fe^{2+}$	W/R 1-10: Fe/Mg smectites, Ca sulfates, Al sulfates, Zeolites W/R 10^3: Fe/Mg smectites, Zeolites W/R 10^6: Oxides
1	1	S(VI) > Cl^- >> C(IV)	W/R 1-10: $Mg^{2+} > Na^+ > Fe^{2+} > Ca^{2+}$ W/R 10^3-10^6: $Mg^{2+} \geq Na^+ \geq Fe^{2+} \geq Ca^{2+}$	W/R 1: Zeolites, Fe sulfates, Ca sulfates W/R 10: Zeolites, Ca sulfates W/R 10^3: Zeolites W/R 10^6: No Minerals

Closed System				
10^{-3}	0.05	C(IV) ≥ S(VI) > Cl^- W/R 10: S(VI) > Cl^- > C(IV)	W/R 0.1: Na^+ >> Fe^{2+} >> Ca^{2+}>> Mg^{2+} W/R 1-10: Na^+ > Ca^{2+} > Fe^{2+} >> Mg^{2+} W/R 10^3-10^6: Mg^{2+} ≥ Ca^{2+} ≥ Na^+ > Fe^{2+}	W/R 0.1-10: Fe/Mg smectites, Ca carbonates W/R 10^3: Fe/Mg smectites, Al phyllosilicates. W/R 10^6: Oxides
1	0.05	W/R 0.1-1: Cl^- > S(VI) > C(IV) W/R 10-10^6: S(VI) > Cl^- >> C(IV)	W/R 0.1: Na^+ > Ca^{2+} >> Fe^{2+} > Mg^{2+} W/R 1: Na^+ > Ca^{2+} >> Mg^{2+} > Fe^{2+} W/R 10-10^6: Mg^{2+} ≥ Fe^{2+} ≥ Na^+ ≥ Ca^{2+}	W/R 0.1: Fe/Mg smectites, Ca/Mg carbonates W/R 1: Fe/Mg smectites, Ca sulfates W/R 10: Ca sulfates, Zeolites W/R 10^3: Zeolites W/R 10^6: No Minerals
10^{-3}	1	C(IV) ≥ S(VI) > Cl^- W/R 10: S(VI) > Cl^- > C(IV)	W/R 0.1: Na^+ >> Fe^{2+} >> Ca^{2+}>> Mg^{2+} W/R 1-10: Na^+ > Ca^{2+} > Fe^{2+} >> Mg^{2+} W/R 10^3-10^6: Mg^{2+} ≥ Ca^{2+} ≥ Na^+ > Fe^{2+}	W/R 0.1-10: Fe/Mg smectites, Pyrite, Ca/Mg/Fe carbonates W/R 10^3: Fe carbonates, Al phyllosilicates, Fe/Mg smectites. W/R 10^6: Oxides
1	1	W/R 0.1-1: Cl^- > S(VI) > C(IV) W/R 10-10^6: S(VI) > Cl^- >> C(IV)	W/R 0.1: Na^+ > Ca^{2+} >> Fe^{2+} > Mg^{2+} W/R 1: Na^+ > Ca^{2+} >> Mg^{2+} > Fe^{2+} W/R 10-10^6: Mg^{2+} ≥ Fe^{2+} ≥ Na^+ ≥ Ca^{2+}	W/R 0.1: Fe/Mg smectites, Ca/Mg carbonates W/R 1: Fe/Mg smectites, Ca sulfates, W/R 10: Ca sulfates, Zeolites W/R 10^3: Zeolites W/R 10^6: No Minerals

333

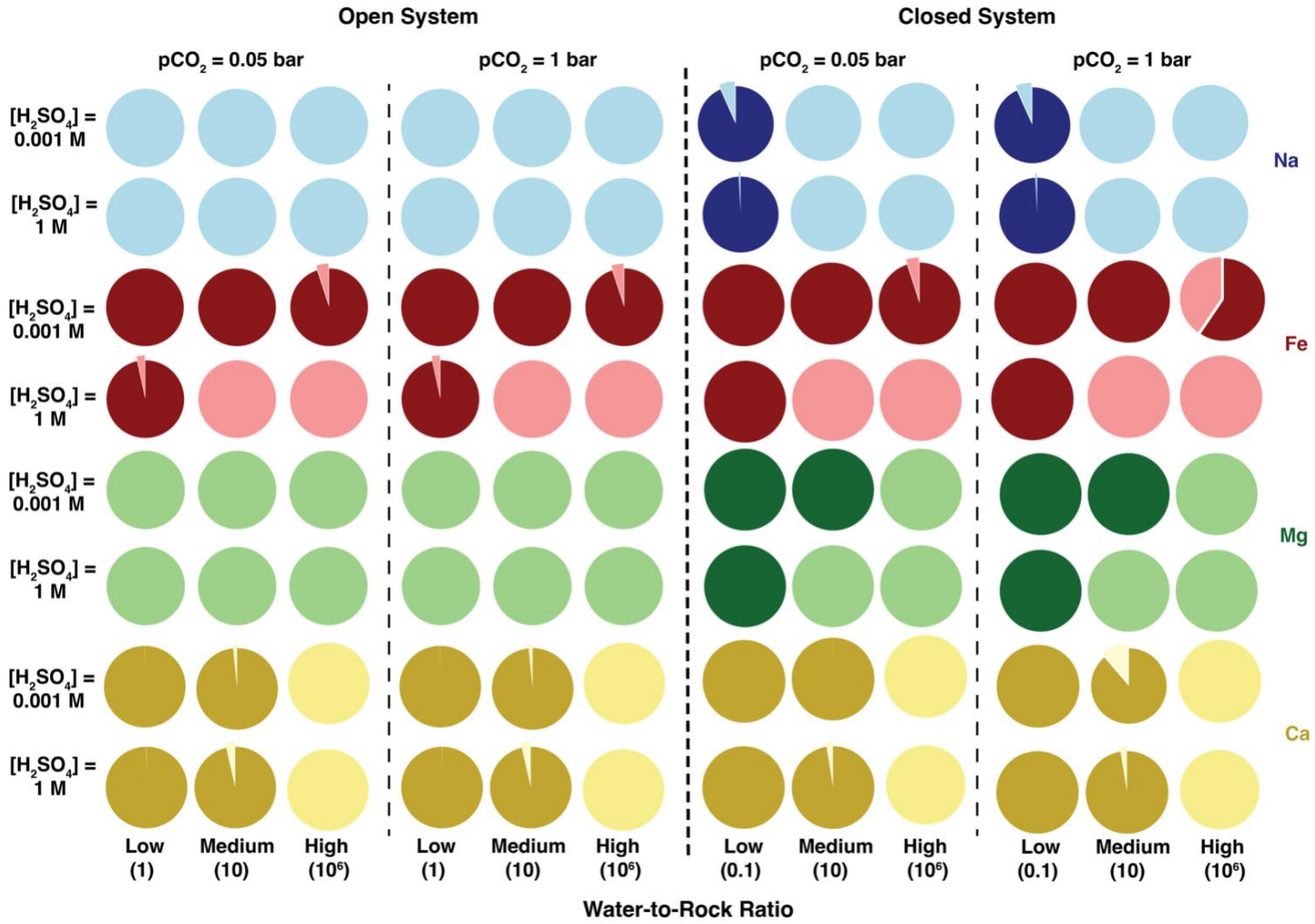

Figure 3: *Pie charts showing proportion of major mineral-forming cations (Fe, Mg, Ca, Na) in mineral vs. leachate at low (1 in open system/0.1 in closed), Medium (10), and high (10^6) W/R and low (10^{-3} mol L^{-1}) and high (1 mol L^{-1}) initial sulfuric acid concentrations at pCO_2 = 0.05 and 1 bar. Left panel shows open system results, while the right panel shows closed system results. Light shades represent the portion in fluid, while darker shade represents the portion in minerals.*

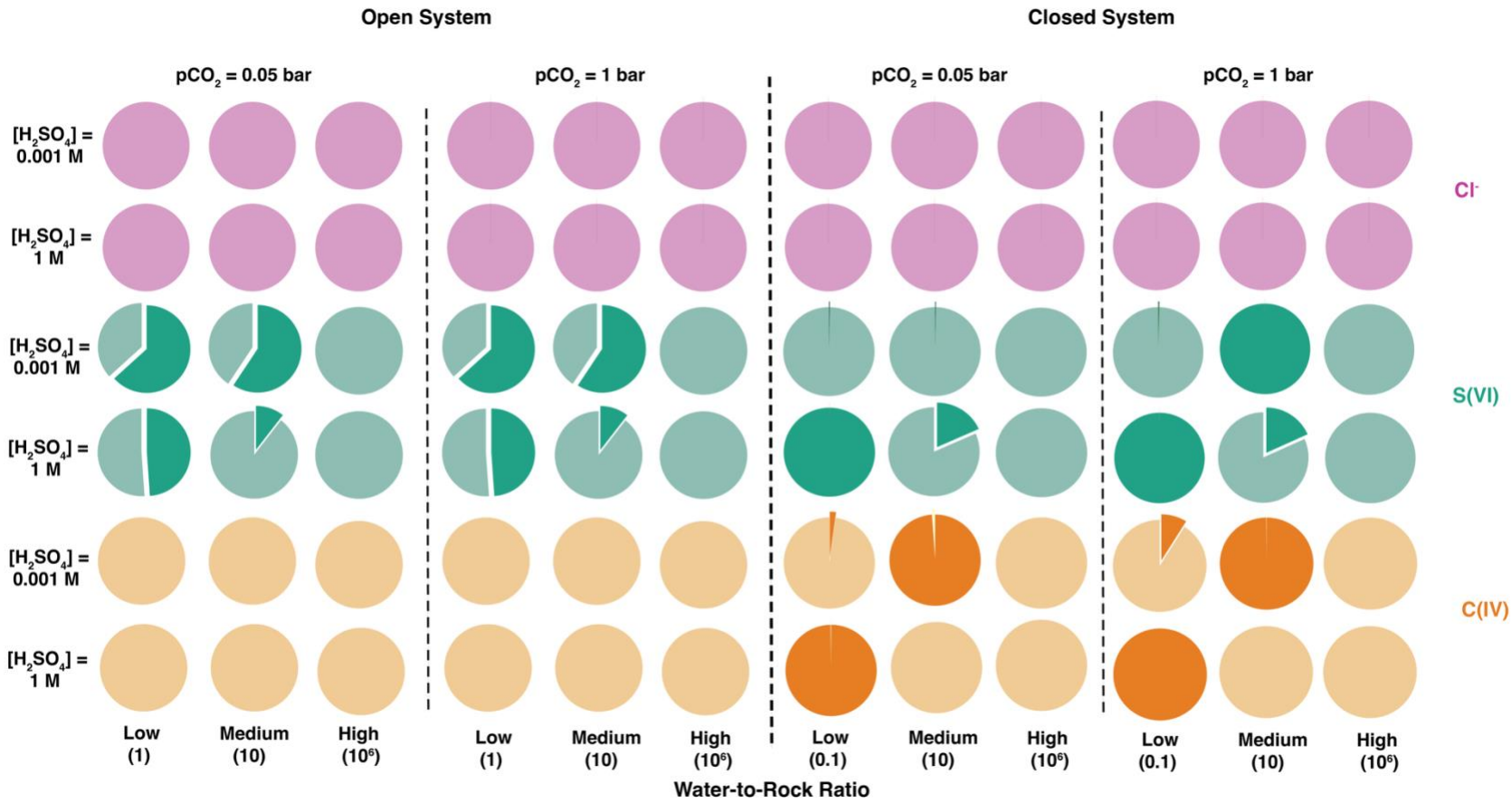

Figure 4: *Pie charts showing proportion of major mineral-forming anions (Cl^-, S(VI), and C(IV)) in mineral vs. Leachate at low (1 in open system/0.1 in closed), Medium (10), and high (10^6) W/R and low (0.001 mol L^{-1}) and high (1 mol L^{-1}) initial sulfuric acid concentration at pCO_2 = 0.05 and 1 bar. Left panel shows open system results, while the right panel shows closed system results. Light shades represent the portion in fluid, while darker shade represents the portion in minerals. Note, despite changing system conditions, Cl^- always remains in fluid.*

3.2 Types of Leachates Produced during Basalt Weathering

3.2.1 Open System

Basalt alteration leachates can be classified and grouped based on the relative abundance of the major anion (SO_4^{2-}, HCO_3^-, Cl^-) and cations (Mg^{2+}, Na^+, Ca^{2+}, Fe^{2+}). The grouping of different leachate types was primarily governed by the initial system acidity (i.e., initial [H_2SO_4]) and the W/R. All leachates produced in the open system were acidic (pH < 4). In open system, we identify three leachate types. At low initial sulfuric acid content conditions ([H_2SO_4] = 10^{-3} mol/L), we identified two types of leachates: an almost pure sulfate leachate at low W/R (1 to 10^3) (Type 1) and a bicarbonate/sulfate-rich leachate at high W/R (10^3 to 10^6) (Type 2) with pH between 4 to 2.5. Type 2 leachate becomes HCO_3^- dominant at high pCO_2 (1 bar). In both these leachate types, Mg^{2+} is the dominant cation with negligible Fe^{2+}.

At high initial sulfuric acid concentration ([H_2SO_4] ≥ 0.5 mol/L), the leachates produced are all highly acidic (pH < 1) and sulfate-rich (Type 3) with relative anion concentrations: SO_4^2 > Cl^- > HCO_3^-. We classify them into three sub-categories based on the variation in relative cation concentrations influenced by the W/R. Although sulfate-rich, the three sub-types of Type 3 leachate are different from type 1 sulfates owing to their substantially higher Fe^{2+} concentrations. At low W/R (~1), the dominant cation is Mg^{2+}, followed by Na^+ and Fe^{2+} (Type 3A Mg Sulfate Leachate). Type 3B leachates have comparable concentrations of Mg^{2+} and Fe^{2+} at W/R ~10. At higher W/R (>10^3), type 3C leachates have almost equal concentrations of Mg^{2+}, Fe^{2+}, and Ca^{2+}.

3.2.2 Closed System

Compared to open systems, the types of leachates produced in closed systems demonstrated greater compositional variability. We identified three leachate types (Type 4, 5, and 6) in low initial sulfuric acid concentration ([H_2SO_4] = 10^{-3} mol/L) conditions. Weathering under a closed system under initially low sulfuric acid content produces bicarbonate-rich leachates (Types 4 and 6) at both low (< 1) and high W/R (>10^3). High pCO_2 conditions promote greater bicarbonate concentration in the leachates. At low W/Rs (~0.1 and 1), highly alkaline, Na bicarbonate leachates (Type 4) are produced. At slightly higher W/R ~10, highly alkaline leachates (type 5) form with high sulfide concentrations and low bicarbonate concentrations at both low and high pCO_2 conditions. At higher W/Rs (>10^3), leachates produced are bicarbonate-rich (Type 6) but differ from Type 4 leachates based on the dominant cation. Type 4 leachates have a single dominant

377 cation, $Na^{+,}$ and have highly alkaline pH (>12), while Type 6 leachates have almost similar
378 concentrations of Na^{+}, Mg^{2+}, and Ca^{2+} with pH between 8 and 3.

379 We have identified two distinct leachate types, an alkaline Na-Cl rich leachate (Type 7)
380 and a highly acidic Mg/Fe sulfate leachate (Type 8), both forming under high initial sulfuric acid
381 content. Basalt weathering under initially highly acidic conditions in a closed, low W/R (< 1) can
382 produce a leachate that is rich in both Na^{+} and Cl^{-}. This is the only sodium and chloride-rich
383 leachate produced in our study. At greater W/Rs (>10), a highly acidic (pH < 2) sulfate-rich
384 leachate containing equal Fe and Mg is produced. Atmospheric pCO_2 does not affect leachate types
385 7 and 8, and bicarbonate concentration in the solution remains low in both leachate types.

386

Table 2: Composition and formation conditions of the different leachate types obtained during basalt weathering and predicted evaporite assemblages.				
Leachate type	**Relative Ionic Composition**	**General Formation Conditions**	**Evaporites** (Predicted in all leachates)	**Evaporites** (Predicted in some leachates)
Open System				
Leachates in Low Initial H_2SO_4 [= 10^{-3} mol/L] Conditions				
Type 1 Mg Sulfate Leachate (very low Fe)	S(VI) >> C(IV) ≥ Cl^- ❖ (S(VI) >> C(IV) + Cl^-) $Mg^{2+} > Na^+ > Ca^{2+} >> Fe^{2+}$	● low W/R (1 to 10^3) ● low and high pCO_2	Gypsum ($CaSO_4.2H_2O$)	Anhydrite ($CaSO_4$) [#40%], Epsomite ($MgSO_4.7H_2O$) [#40%], Glauberite ($Na_2Ca(SO_4)_2$) [#40%], Bloedite ($Na_2Mg(SO_4)_2 \cdot 4H_2O$) [#40%], Rozenite [$Fe^{II}SO_4 \cdot 4H_2O$) [#20%]
Type 2 Ca/Mg-Bicarbonate/Sulfate Leachate	C(IV) ≥ S(VI) > Cl^- $Mg^{2+} \geq Ca^{2+} > Na^+ > Fe^{2+}$	● high W/R (~10^6) ● low and high pCO_2	Siderite ($FeCO_3$)	Gypsum [#66%]
Leachates in High Initial H_2SO_4 Conditions				
Type 3A* Mg Sulfate Leachate	S(VI) > Cl^- > C(IV) $Mg^{2+} > Na^+ > Fe^{2+} >> Ca^{2+}$	● low W/R ~1 ● low and high pCO_2 ● At low pCO_2: $Cl^- >> HCO_3^-$	x	x
Type 3B[$] Mg/Fe Sulfate Leachate	S(VI) > Cl^- > C(IV) $Mg^{2+} \geq Fe^{2+} > Na^+ > Ca^{2+}$	● medium W/R ~10 ● low and high pCO_2		Gypsum [#80%], Siderite [#60%]

Type 3C[$] Sulfate Leachate	S(VI) > Cl^- > C(IV) $Mg^{2+} \geq Fe^{2+} \geq Ca^{2+} > Na^+$	• high W/R >10^3 • low and high pCO_2		Siderite [#12.5%]
Closed System				
Leachates in Low Initial H_2SO_4 [= 10^{-3} mol/L] Conditions				
Type 4[@] Na-bicarbonate Leachate	C(IV) > HS^- > Cl^- $Na^+ >> Fe^{2+} \geq Ca^{2+} >> Mg^{2+}$	• low W/R (0.1 and 1) • Leachates with highest alkalinity (pH > 12) • both low and high pCO_2	Brucite ($Mg(OH)_2$) Halite (NaCl) Portlandite ($Ca(OH)_2$) Chukanovite ($Fe_2(OH)_2CO_3$) Siderite ($FeCO_3$) Calcite ($CaCO_3$) Burkeite ($Na_4(SO_4)(CO_3)$)	
Type 5** Alkaline Leachate	HS^- > Cl^- ≥ C(IV) $Na^+ > Ca^{2+} >> Fe^{2+} >> Mg^{2+}$	• high W/R (~10) • both low and high pCO_2 • Highly alkaline leachates (pH ~ 12)	Calcite Siderite	Portlandite [#50%]
Type 6[$] Bicarbonate Leachate	C(IV) ≥ S(VI) > Cl^- $Mg^{2+} \geq Ca^{2+} \geq Na^+ >> Fe^{2+}$	• high W/R (>10^3) • both low and high pCO_2 • Slightly alkaline to acidic (pH 8 to 3)		Siderite [#50%]
Leachates in High Initial H_2SO_4 [≥ 0.5 mol/L] Conditions				
Type 7	Cl^- >> S(VI) > C(IV) $Na^+ > Ca^{2+} >> Mg^{2+}/Fe^{2+}$	• low W/R (0.1 and 1)	Halite	Portlandite [#88%], Calcite [#88%]Siderite [#88%],

Na-chloride Leachate		• both low and high pCO_2 • Alkaline (pH 9 to 12)		Thenardite [#12%], Glauberite [#12%], Gypsum [#12%], Brucite [#12%]
Type 8$ Mg/Fe Sulfate Leachate	S(VI) > Cl^- > C(IV) $Mg^{2+} \geq Fe^{2+} > Na^+ > Ca^{2+}$	• high W/R (>10) • both low and high pCO_2 • acidic (pH < 2)		Siderite [#40%], Gypsum [#42%], Rozenite [#33%], Szomolnokite [#25%] ($FeSO_4 \cdot H_2O$), Anhydrite [#33%], Epsomite [#8%], Bloedite [#8%], Glauberite [#8%], Halite [#8%], Kieserite [#8%]
*Notes: #Percentages next to evaporite minerals in the 5th column indicate the percent of iterations in which that phase was predicted by models. $Evaporation models for a majority of these iterations ran halfway before the models had to be terminated. @ 75% of evaporation model iterations ran successfully for this leachate type. * Indicates none of the evaporation models ran successfully; ** Only half of the evaporation models ran successfully.*				

387

3.3 Precipitation of Carbonates, Sulfates, and Chlorides: Evaporite Mineral Formation during Leachate Evaporation

The evaporation models predicted minerals that are likely to form upon the evaporation of the leachates. While only eight types of leachates are shown here (Table 2), we modeled the evaporation of all 60 leachates. Open system leachates were all sulfate-rich and, therefore, sulfate salts are expected to form as a result of evaporation or freezing of leachate types 1, 2, and 3. Epsomite ($MgSO_4.7H_2O$), gypsum ($CaSO_4.2H_2O$), and anhydrite ($CaSO_4$) form upon the evaporation of type 1 'Mg-Sulfate leachate' (Table 2). Type 2 'Mg bicarbonate/sulfate' leachate predicted an evaporite assemblage of siderite ($FeCO_3$) and gypsum. Although evaporation of highly concentrated type 3 leachates failed to converge, evaporation of sulfate-rich leachates is most likely to yield sulfate salts (see *section 4.5*). Type 3A 'Mg-sulfate' leachates are most likely to yield a combination of hydrated Mg-sulfate salts upon evaporation or freezing. Type 3B 'Mg/Fe sulfate' and type 3C 'sulfate' leachate could yield a combination of Mg, Fe, and Ca sulfate; the solutions became too complicated and concentrated to model after undergoing about 50% evaporation. Most leachates produced in the open system are depleted in Na^+ and Cl^-, but halite could form as a minor, late-stage product of the evaporation of these leachates.

Compared to open systems, evaporation assemblages produced from closed system leachates (Types 4 to 8) are more diverse. Model evaporation of highly alkaline (pH > 12), type 4 'Na-bicarbonate' leachates produced Mg and Fe hydroxides and carbonates (Table 2); about a quarter of type 4 leachates failed to converge. Halite (NaCl) and burkeite [$Na_4(SO_4)(CO_3)$] could also form. Some Type 5 alkaline leachates upon evaporation produced carbonate minerals and portlandite [$Ca(OH)_2$]. Owing to the lack of relevant thermodynamic data, type 5 leachates, containing high sulfide concentration, failed to converge. Therefore, the absence of evaporitic sulfides prediction in our models cannot entirely preclude their formation. About half of type 6 'bicarbonate leachates' underwent full evaporation and will likely produce carbonate minerals, mainly containing Mg or Ca. The model evaporation of type 7 'Na-chloride leachate' predicted the formation of halite (NaCl). Type 8 'Mg/Fe sulfate leachate' model evaporation failed to converge but would likely produce Mg and Fe sulfate salts upon complete evaporation.

4. Discussion

4.1 System Acidity: The Major Alteration Parameter in Basalt Alteration

Basalt alteration can be thought of as an acid-base neutralization reaction, one in which acidic alteration fluid is being neutralized by ferromagnesian minerals, which act as alkalis. As weathering proceeds, weathering fluid acidity is consumed, thereby increasing its pH. Therefore, basalt weathering is facilitated by an increase in system acidity. The acidity of the starting alteration fluid strongly influences the chemistry of weathering, composition of the leachate, and the mineral assemblages produced upon leachate evaporation (Gislason & Arnorsson, 1993; Tosca et al., 2005; Tosca & McLennan, 2006).

Depending on their initial acidity, alteration fluids could either have high or low 'buffering capacity', which is defined as their mineral dissolution capacity before the solution is buffered to circum-neutral or alkaline pH (Tosca et al., 2005). High buffering capacity fluids have high initial acidity and are typically buffered by the acidic gases in the atmosphere (i.e., open system). These fluids will be able to dissolve a larger amount of ferromagnesian minerals (e.g., olivine, pyroxene) and produce a leachate that has a greater concentration of Fe and Mg in the resulting leachate (Figure 2e to 2h). Low buffering capacity fluids, on the other hand, may have a high initial acid content but fail to maintain their acidity during mineral weathering either due to the lack of constant buffering from the atmosphere or lack of acidic oxides in the atmosphere, or both. The acidity or buffering capacity of the alteration fluid plays a decisive role in basalt alteration on Mars and is a complicated function of system openness, W/R, and atmospheric composition.

4.1.1 System Openness

Weathering fluid acidity is likely influenced the most by system openness. A volcanically active Mars that produces more sulfur- and chlorine-bearing gases could lead to greater acidity of alteration fluids. The accessibility of the weathering system to these gases plays a critical role in determining the initial acidity of the system. An open system, being constantly buffered by the atmosphere, can maintain its acidity (pH < 3.5) even during extensive levels of basalt alteration (Figures 2 and 5). In the open system, weathering occurs entirely under acidic pH, resulting in weathering fluids that are high-buffering-capacity solutions. This is apparent in the fact that our open system simulations generated leachates that were Mg^{2+} and Fe^{2+} dominant and relatively depleted in Ca^{2+} and Na^{+} (Figure 2 and S5).

In closed systems, a larger variation in the fluid pH was observed as the reaction progressed (Figure 5). While the initial pH of closed system weathering fluids were the same as the

corresponding open system fluids, the final pH of the alteration fluids in the closed system were higher due to the consumption of H^+ ions without replenishment in an unbuffered basalt weathering scenario (Figure 5). At circumneutral to alkaline pH conditions, Mg^{2+} and Fe^{2+} are preferentially sequestered into clay minerals and carbonates that deplete these ions in low buffering capacity leachates. Therefore, leachates produced as a result of closed system weathering in low W/R are alkaline and typically rich in Na^+ and Ca^{2+}, compared to Fe^{2+} and Mg^{2+} (Figures 2 and S5). The buffering capacity of closed system fluids increases with greater concentration of acidic gases in the atmosphere and W/R thereby enriching Mg^{2+} and Fe^{2+} concentration in the leachate.

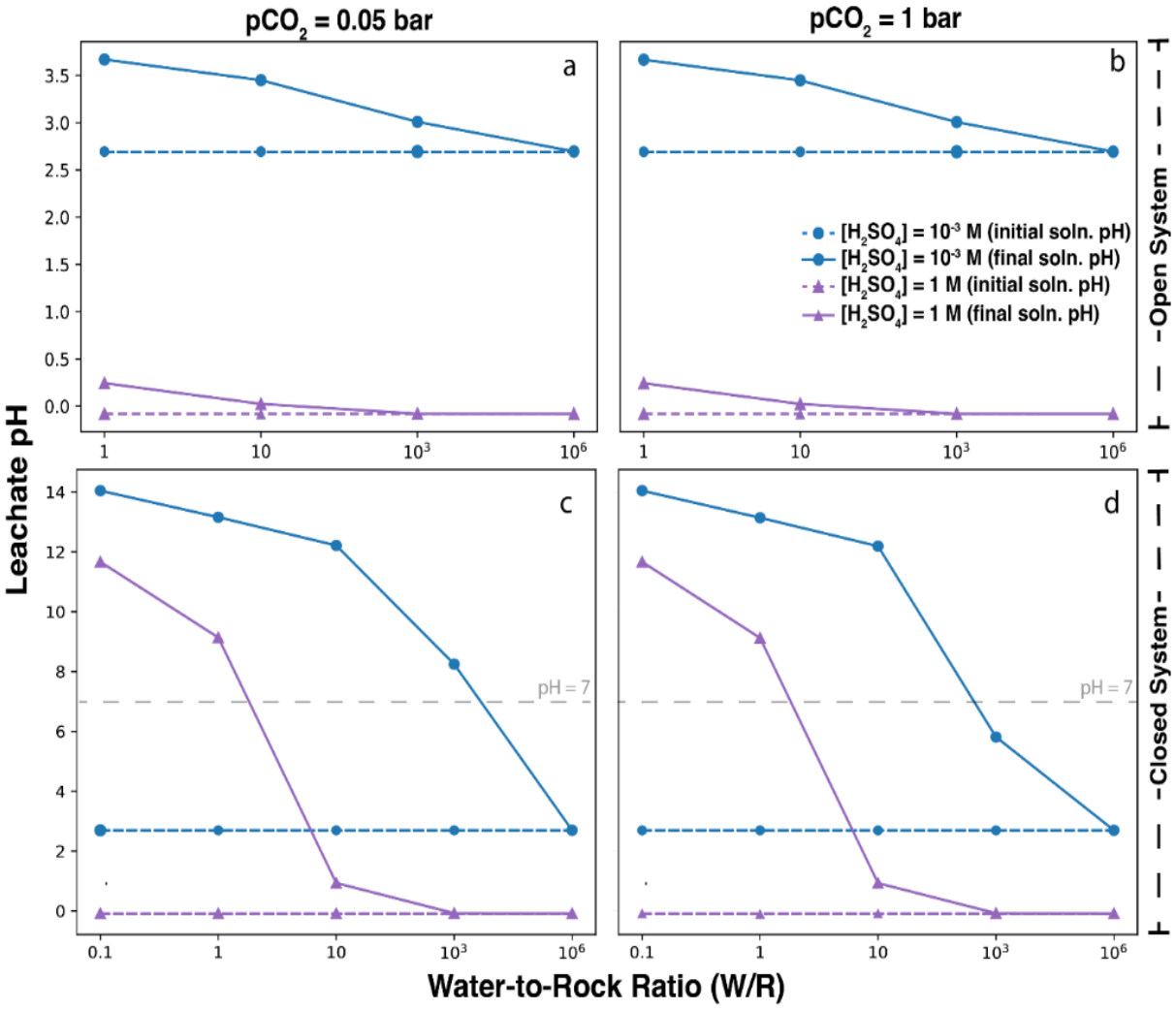

459

460 ***Figure 5:*** *Leachate solution pH at start and end of weathering simulations. pH values are plotted against*
461 *the W/R. Dashed lines connect pH values of initial weathering fluid, and solid lines connect final leachate*
462 *pH after weathering simulation was completed. pH before and after weathering at [H_2SO_4] = 0.001M is*
463 *shown in blue, while pH before and after weathering at [H_2SO_4] = 1M is shown in purple. Open system pH*
464 *values are shown at a) pCO2 = 0.05 bar and b) pCO2 = 1 bar. Closed system pH values are shown at c)*
465 *pCO2 = 0.05 bar and d) pCO2 = 1 bar. Leachate pH is acidic at all modeled conditions for open system*
466 *weathering. Alkaline leachates are generated at lower W/R, particularly at low [H_2SO_4] for closed system*
467 *weathering; however, acidic leachates are generated as W/R is increased.*

468

4.1.2 Effect of atmospheric composition

The concentration and type of gases in the atmosphere and the extent of their dissolution in the fluids determine the initial acidity of the alteration fluids. During quiescent periods, the martian atmosphere would most likely be primarily composed of relatively unreactive gases (N_2, Ar), O_2, H_2, and CO_2 (Wordsworth, 2016). The present thin atmosphere (P_{total} = 6 mbar) of Mars is ~95% CO_2 (Trainer et al., 2019). While it is highly likely that the early Martian atmosphere was thicker (Trainer et al., 2019), its exact composition is speculative. To cover a range of possible scenarios, basalt weathering in our models was conducted under a range of pCO_2 conditions: 0.05 to 1 bar. Similar modeling-based analysis of terrestrial basalts had shown that the amount of CO_2 available in the atmosphere and dissolved in the alteration fluid has a substantial effect on the final mineral products of basalt alteration (S Mitra et al., 2017; Mitra et al., 2018). However, the effect of CO_2 in our models was less intense, likely due to the presence of other acidic gases that produce stronger acids than H_2CO_3.

Sulfur- and chlorine-containing gases are important volcanic gases on Mars. An intense phase of volcanic activity on Mars can degas large amounts of acidic gases into the atmosphere that would then substantially influence the surface geochemistry on the planet, including basalt weathering (Tosca et al., 2004; Hurowitz et al., 2014; Halevy & Head, 2014; Bellino & Sun, 2025). The dissolution of these acidic gases, and their oxidized products, has a substantial effect on fluid acidity as they can form strong acids, such as sulfurous [H_2SO_3], sulfuric [H_2SO_4], and hydrochloric [HCl] acids (Halevy & Head, 2014; Bellino & Sun, 2025). These acids exert a major control on the acidity of the system, thereby controlling the extent of basalt alteration and its alteration products. The major anions of the leachates produced were primarily a function of atmospheric gases. At least four out of the eight different leachate types produced at the end of basalt alteration are sulfate-rich; two other leachate types were bicarbonate-rich, while one was rich in chloride. The evaporite minerals produced due to leachate evaporation are, therefore, a strong function of the atmospheric gas composition. The amount of gases dissolved is also dependent on the amount of water available, which is controlled by W/R.

4.1.3 Water-to-Rock Ratio (W/R)

W/R substantially controls system acidity and therefore exerts a major influence on the extent of basalt alteration and its products, both mineral and fluid. W/R is a measure of the amount

of weathering fluid available and therefore determines the total amount of dissolved acidic gases available for basalt alteration. A greater W/R under any geochemical scenario will increase the total acidity available to interact with the rock. While pH is dependent on the atmospheric composition and independent of the amount of fluid, the buffering capacity of the alteration fluid increases with W/R as it leads to larger amounts of fluid available for weathering. Due to the relatively greater amount of H^+ available in systems with large W/R, the change in pH of the alteration fluid is lower than those with a lower amount of alteration fluid (Figures 2 and 5). At lower W/R, weathering fluid pH rises substantially as weathering continues, resulting in leachates with alkaline pH (Figure 5). Depending on the initial acidity of the alteration fluid, alkaline leachates can also be produced at moderate/high W/R (10-10^3) (Figure 5). However, under volcanically active and high-water availability conditions, the leachates produced are acidic owing to the high buffering capacity of the alteration fluids.

Aside from the pH, W/R determines the concentration of all dissolved components of the leachates. Ions released into the solution during weathering could precipitate as minerals if saturated. Mineral saturation at a given temperature is controlled by the ion activities of the individual mineral component (e.g., Na^+ and Cl^- in halite), which is controlled by the amount of water available. Primary mineral precipitation is, therefore, more likely at lower W/R when minerals can reach saturation owing to greater concentration of dissolved cations and anions. In weathering systems, the total amount of dissolved components increases with increasing W/R due to greater basalt alteration; however, the ionic concentrations of leachates are invariably lower at very high W/R (~10^6) when compared to their lower counterparts (~1).

4.2 Geochemical Constraints on the Formation of Chloride Salts on Mars

Chlorides are different from other salt deposits (i.e., sulfates and carbonates) found on the surface of Mars. Firstly, it is highly likely that all chloride salts on Mars are primarily sodium-bearing, either halite (NaCl) or hydrohalite ($NaCl.2H_2O$) (Bridges & Grady, 2000; Glotch et al., 2016; Thomas et al., 2019). Contrary to halite, multiple cations are associated with sulfate and carbonate salts on Mars, including sodium, calcium, iron, and magnesium (Ehlmann & Edwards, 2014; Hazen et al., 2023). Secondly, the element chlorine is in its lowest possible oxidation state (-1) as chloride (Cl^-) anion, while both sulfur and carbonate exist in their highest oxidation states of +6 and +4 as oxyanions, sulfate ($S^{+VI}O_4^{2-}$) and carbonate ($C^{+IV}O_4^{2-}$), respectively. Chlorine

atoms can also exist in higher oxidation states when present as oxychlorine salts, such as perchlorate ($Cl^{+VII}O_4^-$) and chlorate ($Cl^{+V}O_3^-$), but chloride (Cl^-) salts represent the dominant chlorine-bearing salt on Mars primarily owing to their greater stability (Mitra, 2025). Third, halite salts are produced exclusively via evaporation, unlike sulfate and carbonate, which may also be produced as an alteration mineral product of basalt weathering; however, hydrohalite salts have been proposed to also form by the hydration of halite salts or brine freezing (Hazen et al., 2023).

Owing to their high solubility, chloride salts are often produced only in the last stages of fluid evaporation. Therefore, chloride salt detection on Mars indicates the last vestiges of evaporating brines before it experienced complete desiccation. Multiple chloride salt formation hypotheses in a variety of geological environments have been proposed: ponding and evaporation of surface water runoff and/or upwelled groundwater, formation in shallow lacustrine environments (Osterloo et al., 2008; 2010, Ruesch et al., 2012; El-Maary et al., 2013), deep lake environments (Hynek et al., 2015), shallow ponding related to episodic obliquity change-induced meltwater runoff during late-Hesperian to Early Amazonian (Melwani-Daswani & Kite, 2017; Leask & Ehlmann, 2022), shallow playa lake environments (Glotch et al., 2016), diagenetic or hydrothermal brine systems, and efflorescence (Osterloo et al., 2008; 2010). These studies have proposed chloride depositional scenarios largely based on remote sensing observations, but a thorough geochemical consideration for the formation and evaporation of specific brines/leachates has been lacking.

Using our geochemical models we can constrain the type of leachates and the geochemical conditions required for chloride deposits on Mars. Only a narrow range of conditions is favorable for the formation of chloride-dominated leachates, which, upon evaporation (or freezing), could produce chloride deposits. Additionally, out of the eight leachate types identified in our analysis (Table 2), only leachate type 7 has been classified to be rich in sodium chloride containing sodium (Na^+) and chloride (Cl^-) as the dominant cation and anion pair. Neither sodium nor chlorine was dominant in leachates formed under open system weathering conditions. Closed system leachates are more compositionally diverse, but most were depleted in chloride. While sodium became the dominant cation in other leachate types in closed system weathering, chloride was dominant only in leachate type 7 where the leachate was highly acidic and at low W/R (<=1) ratio (Figure S2).

Evaporation of type 7 leachate produced halite (NaCl) as the major product in the evaporite assemblage. Other evaporite minerals produced along with halite include sulfates and carbonates;

however, their relative abundances are minor compared to halite. Complete evaporation of 'Na-bicarbonate' leachate type 4 and 'Mg/Fe sulfate' leachate type 8 likely produces minor amounts of sodium chloride along with carbonate and sulfate salts. While formation of minor amounts of halite is possible in other leachates, only type 7 leachates produce halite as the dominant evaporite mineral.

The formation of type 7 'sodium chloride' leachates requires closed system basalt weathering conditions under high initial acidity ($[H_2SO_4] \geq 0.5$ mol/L) and low W/R (≤ 1); atmospheric CO_2 seems to have little to no effect on the composition of NaCl leachates. An open system weathering condition in which the alteration fluid is buffered by the atmosphere fails to produce a leachate that is capable of producing even minor amounts of sodium chloride. Only when a small amount of alteration fluid (W/R $\leq$ 1), produced during high volcanic activity, interacts with the Martian basalt in a closed system, can a leachate rich in both Na^+ and Cl^- be produced, which, upon evaporation, predominantly produces halite. These conditions are consistent with a relatively dry Noachian-Hesperian Mars where substantial acidic input could be derived from volcanic degassing (Head et al., 2006; Halevy & Head, 2014; Wordsworth et al., 2021; Kite & Conway, 2024). Thus, a specific, narrow range of highly acidic and water-limited closed-system condition is favorable for leachates that can produce chloride deposits on Mars.

4.3 Evaporative Production of Carbonates on Mars

Carbonate minerals on Mars can form via both primary and secondary mineralization pathways (Hazen et al., 2023). Primary mineralization of Fe-Mg-Ca carbonate phases from aqueous phases can occur in hydrothermal systems (Osinksi et al., 2013; Ojha et al., 2021), during chemical precipitation or authigenesis (Tosca and McLennan, 2006; Leask and Ehlmann, 2022; Morris et al., 2010; Tosca et al., 2018; Bristow et al., 2021; Mojzsis and Arrhenius, 1998; Adcock et al., 2013; Horgan et al., 2020), during evaporation, and freezing of leachates (Payré et al., 2020; Cox et al. 2022). Considering the possibility of relatively long-lived, alkaline lakes on Mars (Hurowitz et al., 2023), the chemical precipitation of authigenic carbonate minerals in crater lakes is likely (Horgan et al., 2020). Fe-Mg-Ca carbonates, along with other authigenic minerals, can also form by the evaporation (or freezing) of leachates produced at the end of basalt alteration.

Carbonate deposits on the surface of Mars have mostly remained elusive. Small amounts of carbonates have been detected in unaltered Martian meteorites and on the surface of Mars via

593 lander, rover, and orbiter instruments. Based on mostly orbital data, solid solutions of Fe-Mg-Ca
594 carbonates have been proposed on the surface of Mars (Boynton et al., 2009; Bridges et al., 2019;
595 Clavé et al., 2023; Ehlmann et al., 2008; Harvey and McSween, 1996; Morris et al., 2010; Niles et
596 al., 2013; Zastrow and Glotch, 2021). The different types of carbonates detected or inferred on
597 Mars include: ankerite [$CaFe(CO_3)_2$] (Rubin and Ma, 2021; Thorpe et al., 2022), aragonite
598 [$CaCO_3$] (Meyer, 2012), calcite [$CaCO_3$] (Rubin and Ma, 2021), dolomite [$CaMg(CO_3)_2$] (Tirsch
599 et al., 2018; Harvey and McSween, 1996), magnesite [$MgCO_3$] (Rubin and Ma, 2021; Bandfield
600 et al., 2003; Ehlmann et al., 2009), and siderite [$FeCO_3$] (Piercy et al., 2022; Thorpe et al., 2022;
601 Tutolo et al., 2025).

602 Out of the eight different leachate types identified in our study, three were bicarbonate-
603 rich: type 2, type 4, and type 6 leachates. According to the evaporation models, the main carbonate
604 phase produced by either partial or complete evaporation of Types 2, 4, and 6 leachate was siderite
605 [$FeCO_3$]. Calcite [$CaCO_3$], chukanovite [$Fe_2(OH)_2CO_3$], and burkeite [$Na_4(SO_4)(CO_3)$] were also
606 predicted upon evaporation of bicarbonate-rich leachates but in relatively minor proportion (Table
607 2). In addition to bicarbonate-rich leachate types, other leachates in our study also produced
608 carbonate minerals upon evaporation. Siderite was produced along with other evaporite minerals
609 in type 3B 'Mg/Fe sulfate', 3C 'sulfate', 5 'Na/Ca sulfate', 7 'Na chloride', and 8 'Mg/Fe sulfate'
610 leachates; calcite [$CaCO_3$] precipitation was predicted by the evaporation of leachate type 4, 5,
611 and 7. Magnesite [$MgCO_3$] precipitation was not predicted to form in any leachate type which
612 could be attributed to the greater hydration of Mg^{2+} ions.

613 Recently, large deposits of pure, crystalline iron carbonate mineral siderite [$FeCO_3$] were
614 detected in the sulfate-rich Mirador formation at Gale crater, Mars (Tutolo et al., 2025). Along
615 with 4-10 wt.% of siderite, the drill samples of Tapo Caparo (TC), Ubajara (UB), and Sequoia
616 (SQ) contain a combination of Ca and Mg-sulfate minerals from 0.5 to 6 wt.%. %. Ca-sulfate
617 minerals detected along with siderite are anhydrite [$CaSO_4$], bassanite [$CaSO_4.0.5H_2O$], and
618 gypsum [$CaSO_4.2H_2O$]. The Mg-sulfate minerals detected in the TC, UB, and the SQ drill samples
619 include mutually exclusive starkeyite [$MgSO_4.4H_2O$] or kieserite [$MgSO_4.H_2O$]. Because the
620 crystalline siderite found was almost pure Fe (97-100%) end member, the carbonate was likely not
621 produced as a secondary mineral product by ferromagnesian mineral alteration. Pure siderite was
622 likely produced from the authigenic precipitation from a solution containing dissolved Fe^{2+} and
623 carbonate anion (Tutolo et al., 2025), similar to those predicted in our study.

Siderite was proposed to be the first mineral precipitating out from the evaporation (or freezing) of a basalt dissolution leachate, followed by the precipitation of Ca-sulfate phases (gypsum or anhydrite) and eventually Mg-sulfate (meridianiite, epsomite, or kieserite). However, the composition of the leachate and the conditions of basalt alteration were not proposed (Tutolo et al., 2025). The evaporation of Mg/Fe sulfate leachate types 3B and 8 can both lead to the formation of siderite along with Ca- and Mg-sulfates; leachate type 2 also produces siderite and Ca-sulfates without the formation of any Mg-sulfate phase. Types 3B and 8 are both Mg/Fe sulfate leachates that are highly likely to produce a combination of siderite, gypsum, anhydrite, and epsomite upon evaporation; bassanite and anhydrite can form either directly during late-stage evaporation of the leachates or by the dehydration of gypsum. It is important to note that the assemblage of siderite and Ca/Mg sulfates was not produced by the evaporation of a carbonate-rich leachate but instead from a 'sulfate-rich' leachate. The high acidity of type 8 leachate may lead to siderite dissolution, but a recent experimental study pointed out the stability of siderite in highly acidic fluids (Mitra et al., 2025).

The two leachates that are likely to produce siderite with Ca- and Mg-sulfate salts upon evaporation, 3A and 8, were both Mg/Fe sulfate leachates produced during chemical weathering of basalt in open and closed system conditions, respectively. Both leachate types are possible between 0.05 to 1 bar pCO_2 but require high initial acidity ($[H_2SO_4] > 0.5$ mol/L). Therefore, an evaporite assemblage containing both $FeCO_3$ and Ca/Mg-sulfate is not only possible on volcanically active Mars but may be a necessity to explain the recent siderite detection at Gale crater. Maintaining an optimal concentration of carbonate, sulfates, and the dissolved cations is likely important, which is possible in medium W/R (~10) in open systems but requires high W/R (>10) in closed system weathering.

4.4 Evaporative Production of Sulfates on Mars

Sulfate salts are abundant on the surface of Mars (Ehlmann and Edwards, 2014). More than 20 different varieties of sulfates have either been identified or inferred to be present on the Martian surface, including Ca, Mg, Na, and Fe sulfates and their hydrates (e.g., Benison, 2016; Bishop et al., 2009; Farrand et al., 2009, 2014; Hazen et al., 2023; Klingelhöfer et al., 2004; Morris et al., 2008; Rice et al., 2010; Vaniman et al., 2018; Wang et al., 2006; Vaniman et al. (2018); Burt et al. 2011; Farrand et al., 2014; Wang et al., 2009; Klingelhöfer et al., 2004; Farrand et al., 2009;

Gendrin et al., 2005; Peterson et al., 2007; Pitman et al., 2014). Sulfate salts can form via both primary and secondary mineralization pathways: vapor-phase deposition during volcanic eruption, hydrothermal (Berger et al., 2017; Nachon et al., 2014; Schwenzer et al., 2016), authigenic primary precipitation (Blake et al., 2013; Klingelhöfer et al., 2004; Morris et al., 2008, 2019; Rampe et al., 2017, 2018; Rampe, Blake, et al., 2020; Rampe, Bristow, et al., 2020; Thorpe et al., 2022; Treiman et al., 2016; Vaniman et al., 2014; Farrand et al., 2009; Mitra et al., 2019, 2020, 2022), hydration/dehydration of existing sulfates (Chipera & Vaniman, 2007; Peterson et al., 2007; Wang et al., 2006, 2009, 2011), oxidation of Fe(II)-bearing minerals (Mitra et al., 2023), and diagenesis (Aubrey et al., 2006; Farrand et al., 2009; Gendrin et al., 2005; Morris et al., 2007; Vaniman et al., 2004; Wang et al., 2006, 2009, 2011; Wray et al., 2009). While several sulfate minerals were produced as a product of basalt weathering, here we focus on sulfate minerals produced by evaporation of sulfate leachates. About half of the leachates identified in our study were classified as sulfate rich. Almost all leachates produced from basalt weathering in open systems were sulfate rich leachates containing different compositions of cations that were controlled by the buffering capacity of the alteration fluid. Alteration fluids that started with high initial acidity ($[H_2SO_4] >= 0.5$ mol/L) in an open system, produced Mg- (type 3A) and Mg/Fe-rich sulfate leachates (type 3B) at low (W/R ~1) and moderate (~10) W/R. While type 3A leachates, when evaporated in our models, failed to converge owing to their high ionic strength, we predict the formation of Mg-sulfate salts, mainly epsomite [$MgSO_4.7H_2O$] upon its evaporation; subsequent dehydration could produce starkeyite [$MgSO_4.4H_2O$] and kieserite [$MgSO_4.H_2O$]. Evaporation models predicted gypsum precipitation upon evaporation of ~80% leachates of type 3B. Precipitation of Mg/Fe/Ca sulfates is possible in leachate types 3B and 3C, given their relative abundance in the fluid (Table 2).

In leachates produced under low initial sulfuric acid content ($[H_2SO_4] < 10^{-3}$ mol/L) in the open system, gypsum was predicted to be a major sulfate phase produced upon leachate evaporation. Type 1 leachate produced a variety of other sulfate phases, including anhydrite, epsomite, glauberite, bloedite, and rozenite. Evaporation of leachates produced under closed system weathering can also produce evaporative sulfates. Type 8 'Mg/Fe Sulfate' leachate upon evaporation could produce a mixture of sulfate salts containing gypsum, rozenite, szomolnokite, anhydrite, epsomite, bloedite, glauberite, and kieserite. Interestingly, type 7 'sodium chloride' leachate could also produce minor quantities of gypsum, thenardite, and glauberite. Therefore, a

686 wide variety of sulfate deposits on Mars could be the result of evaporation of basalt alteration
687 leachates.

688 Ferric minerals, such as jarosite and schwertmannite, were not predicted in our models.
689 Therefore, a low pO_2 (= 0.05 bar) atmosphere is likely unable to produce ferric [Fe(III)] sulfates
690 and likely requires either greater amount of O_2 or stronger oxidants. Reactive oxyhalogen salts,
691 such as chlorate [ClO_3^-] and bromate [BrO_3^-], can effectively oxidize dissolved ferrous iron [Fe(II)]
692 and ferrous sulfide minerals (e.g., pyrite [FeS_2], pyrrhotite [$Fe_{1-x}S$]) under Mars-relevant
693 conditions and produce ferric hydroxysulfate minerals, jarosite, and schwertmannite (Mitra et al.,
694 2023).
695
696 ***4.5 Limitations of Geochemical Modeling and Need for Future Work***

697 The database used in our study contains thermodynamic data for about 1200 mineral
698 species at 25°C. While other available thermodynamic datasets, such as the *thermo_minteq*,
699 contain thermodynamic data between 0 and 100°C, they are substantially limited in terms of the
700 number of aqueous and mineral species. In this study, we have chosen the greater diversity in
701 database over low-temperature geochemical modeling below 25°C. Investigation using databases
702 with thermodynamic data at higher and lower temperatures will likely increase our understanding
703 of basalt alteration in hydrothermal and colder conditions on Mars. Another common limitation in
704 most thermodynamic databases is the inability to simulate fluid behavior and evolution in high
705 ionic strength fluids. While we used a database that has Pitzer parameters for common dissolved
706 ions present in natural waters, a few of our leachates upon substantial evaporation failed to
707 converge before reaching complete evaporation. Laboratory investigation of leachate fluid
708 evolution is warranted to validate our mineral precipitation predictions in these fluids.

709 In this study, we conducted purely thermodynamic modeling. Kinetically inhibited mineral
710 and aqueous phases under our reaction conditions were suppressed (Supplementary Section S1) to
711 account for simple kinetic inhibitions factors during basalt weathering. However, kinetic and
712 reactive transport modeling can provide additional information about the rates of reaction,
713 alteration fluid movement, and the formation of alteration phases as a function of depth. Therefore,
714 additional kinetic modeling studies and analogous experimental investigation are essential to better
715 understand basalt weathering on the surface and sub-surface of Mars.

716 The choice of model parameters, although extensive in our study, could be further
717 expanded to include the variability of atmospheric oxygen and other oxidants (chlorate, UV rays)
718 present on the surface of early or modern Mars. The increased availability of oxidants in basalt
719 alteration systems is likely to play an important role in determining the fate of redox sensitive
720 elements, such as iron, by producing more ferric minerals than observed in our modeling. Future
721 investigations of basalt alteration on Mars would benefit from focusing on modeling basalt
722 alteration containing greater influence of oxidants.
723
724 **5. Conclusion**
725 In this modeling study, we investigated leachates produced during basalt alteration under
726 diverse physicochemical conditions plausible on early Mars. Aqueous alteration of basalt under a
727 variety of geochemical conditions demonstrates the formation of at least eight different types of
728 leachates that can produce primary evaporite minerals containing chlorides, carbonates, or sulfate
729 salts on Mars. Sulfate-rich leachates (types 1, 2, 3, and 8) were the most common, typically formed
730 under highly acidic conditions. Gypsum [$CaSO_4.2H_2O$] was the primary evaporite produced and
731 Mg, Fe, and Na sulfates salts were also predicted. While possible under closed system weathering,
732 evaporative sulfates were predominant under open system weathering.
733 Evaporative carbonates were produced along with sulfates from leachates produced under
734 both open and closed system alteration. All fluids of type 2 and 4 leachates produced a combination
735 of Fe and Ca carbonates along with gypsum. Siderite [$FeCO_3$] was the dominant carbonate phase
736 since Ca is precipitated as sulfate (gypsum) as well as carbonate (calcite) salts; Mg-carbonates
737 were not predicted under any alteration condition. Evaporative formation of siderite likely requires
738 an alkaline to near-neutral leachate that was produced by closed system basalt weathering under
739 low initial sulfuric acid ($[H_2SO_4] \leq 10^{-3}$ mol/L) concentration (leachate types 4, 5, and 6). While
740 leachates characterized primarily as 'sulfate-rich' can also produce siderite, only bicarbonate-rich
741 leachates can produce carbonates as the major evaporite. While atmospheric pCO_2 did not play a
742 substantial role in determining evaporative siderite formation, system acidity, which is controlled
743 by initial sulfuric acid concentration, water-to-rock ratio, and system openness, exerts a major
744 control on evaporative siderite formation. Siderite precipitation in evaporating sulfate-rich acidic
745 fluids is theoretically possible but requires experimental validation.
746 Contrary to sulfates and carbonates, chloride precipitation was constrained in leachates
747 produced under specific basalt alteration conditions: closed system environment with high initial

748 sulfuric acid content at low W/R. Halite (NaCl) precipitated as the major evaporite from type 7
749 'sodium chloride' leachate; minor amounts of NaCl is possible upon complete evaporation of type
750 4 bicarbonate-rich leachates. Additionally, only sodium (Na) chloride precipitated in our models;
751 Mg, Ca, and Fe chloride salts are therefore unlikely to form as evaporites on the surface of Mars.
752 Chloride-bearing outcrops on Mars, with typical ages ~3.6 to 2.3 Ga, are therefore halite deposits
753 that were likely produced by evaporation of leachates produced during volcanically active yet
754 water-limited conditions on Mars.

Data Availability: GWB React run files for first open system and closed system leaching and evaporation models, a spreadsheet containing the full description of model workspace parameters used for each iteration, and the resulting data from models used in our analyses are available on our Zenodo repository (Das, Mitra 2026).

Acknowledgements: This work was supported by a NASA PSD Future Investigators in NASA Earth and Space Science and Technology (FINESST) grant (NNH23ZDA001N): 23-PLANET23-0056 awarded to E. Das, T. D. Glotch, and K. Mitra. KM also acknowledges support from UT San Antonio. We would like to thank A. Mukherjee for assistance with modeling work. We would like to thank S. M. McLennan for valuable discussion and feedback on this work.

Appendix A. Supplementary Material: Supplementary Materials contain Sections S1-2 providing descriptions of suppressed phases, and k-means clustering; Table S1 containing substrate composition; and Figures S1-S5 which show leachate compositions.

Conflict of Interest Statement:

The authors declare no conflict of interest relevant to this study.

References:

Adcock, C. T., Hausrath, E. M., & Forster, P. M. (2013). Readily available phosphate from minerals in early aqueous environments on Mars. *Nature Geoscience*, *6*(10), 824–827. https://doi.org/10.1038/ngeo1923

Aubrey, A., Cleaves, H. J., Chalmers, J. H., Skelley, A. M., Mathies, R. A., Grunthaner, F. J., et al. (2006). Sulfate minerals and organic compounds on Mars. *Geology*, *34*(5), 357–360. https://doi.org/10.1130/G22316.1

Bandfield, J. L., Glotch, T. D., & Christensen, P. R. (2003). Spectroscopic Identification of Carbonate Minerals in the Martian Dust. *Science*, *301*(5636), 1084–1087. https://doi.org/10.1126/science.1088054

Bellino, L. G., & Sun, C. (2025). Volcanic emission of reduced sulfur species shaped the climate of early Mars. *Science Advances*, *11*(36), eadr9635. https://doi.org/10.1126/sciadv.adr9635

Benison, K. C. (2016). Alunite on Mars. *American Mineralogist*, *101*(7), 1499–1500. https://doi.org/10.2138/am-2016-5802

Benison, K. C., Gill, K. K., Sharma, S., Siljeström, S., Zawaski, M., Bosak, T., et al. (2024). Depositional and Diagenetic Sulfates of Hogwallow Flats and Yori Pass, Jezero Crater: Evaluating Preservation Potential of Environmental Indicators and Possible Biosignatures From Past Martian Surface Waters and Groundwaters. *Journal of Geophysical Research: Planets*, *129*(2), e2023JE008155. https://doi.org/10.1029/2023JE008155

Berger, J. A., Schmidt, M. E., Gellert, R., Boyd, N. I., Desouza, E. D., Flemming, R. L., et al. (2017). Zinc and germanium in the sedimentary rocks of Gale Crater on Mars indicate hydrothermal enrichment followed by diagenetic fractionation. *Journal of Geophysical Research: Planets*, *122*(8), 1747–1772. https://doi.org/10.1002/2017JE005290

Bethke, C. M. (2022). *Geochemical and Biogeochemical Reaction Modeling* (3rd ed.). Cambridge: Cambridge University Press. https://doi.org/10.1017/9781108807005

Bibring, J.-P., Langevin, Y., Mustard, J. F., Poulet, F., Arvidson, R., Gendrin, A., et al. (2006). Global Mineralogical and Aqueous Mars History Derived from OMEGA/Mars Express Data. *Science*, *312*(5772), 400–404. https://doi.org/10.1126/science.1122659

Bishop, J. L., Parente, M., Weitz, C. M., Noe Dobrea, E. Z., Roach, L. H., Murchie, S. L., et al. (2009). Mineralogy of Juventae Chasma: Sulfates in the light-toned mounds, mafic minerals in the bedrock, and hydrated silica and hydroxylated ferric sulfate on the plateau. *Journal of Geophysical Research: Planets*, *114*(E2). https://doi.org/10.1029/2009JE003352

Blake, D. F., Morris, R. V., Kocurek, G., Morrison, S. M., Downs, R. T., Bish, D., et al. (2013). Curiosity at Gale Crater, Mars: Characterization and Analysis of the Rocknest Sand Shadow. *Science*, *341*(6153), 1239505. https://doi.org/10.1126/science.1239505

Blanc, Ph., Lassin, A., Piantone, P., Azaroual, M., Jacquemet, N., Fabbri, A., & Gaucher, E. C. (2012). Thermoddem: A geochemical database focused on low temperature water/rock interactions and waste materials. *Applied Geochemistry*, *27*(10), 2107–2116. https://doi.org/10.1016/j.apgeochem.2012.06.002

Boynton, W. V., Ming, D. W., Kounaves, S. P., Young, S. M. M., Arvidson, R. E., Hecht, M. H., et al. (2009). Evidence for Calcium Carbonate at the Mars Phoenix Landing Site. *Science*, *325*(5936), 61–64. https://doi.org/10.1126/science.1172768

Bridges, J. C, & Grady, M. M. (2000). Evaporite mineral assemblages in the nakhlite (martian) meteorites. *Earth and Planetary Science Letters*, *176*(3), 267–279. https://doi.org/10.1016/S0012-821X(00)00019-4

Bridges, John C., Hicks, L. J., & Treiman, A. H. (2019). Chapter 5 - Carbonates on Mars. In J. Filiberto & S. P. Schwenzer (Eds.), *Volatiles in the Martian Crust* (pp. 89–118). Elsevier. https://doi.org/10.1016/B978-0-12-804191-8.00005-2

Bristow, T. F., Grotzinger, J. P., Rampe, E. B., Cuadros, J., Chipera, S. J., Downs, G. W., et al. (2021). Brine-driven destruction of clay minerals in Gale crater, Mars. *Science*, *373*(6551), 198–204. https://doi.org/10.1126/science.abg5449

Buz, J., Ehlmann, B. L., Pan, L., & Grotzinger, J. P. (2017). Mineralogy and stratigraphy of the Gale crater rim, wall, and floor units. *Journal of Geophysical Research: Planets*, *122*(5), 1090–1118. https://doi.org/10.1002/2016JE005163

Catalano, J. G. (2013). Thermodynamic and mass balance constraints on iron-bearing phyllosilicate formation and alteration pathways on early Mars. *Journal of Geophysical Research: Planets*, *118*(10), 2124–2136. https://doi.org/10.1002/jgre.20161

Catling, D. C., Claire, M. W., & Zahnle, K. J. (2015). Volatiles and Habitability. In B. Schubert (Ed.), *Treatise on Geophysics* (2nd ed., Vol. 10, pp. 177–210). Elsevier.

Chipera, S. J., & Vaniman, D. T. (2007). Experimental stability of magnesium sulfate hydrates that may be present on Mars. *Geochimica et Cosmochimica Acta*, *71*(1), 241–250. https://doi.org/10.1016/j.gca.2006.07.044

Clark, J. V., Sutter, B., McAdam, A. C., Knudson, C. A., Casbeer, P., Tu, V. M., et al. (2024). Hydrogen Chloride and Sulfur Dioxide Gas Evolutions from the Reaction between Mg Sulfate and NaCl: Implications for the Sample Analysis at the Mars Instrument in Gale Crater, Mars. *Minerals*, *14*(3), 218. https://doi.org/10.3390/min14030218

Clavé, E., Benzerara, K., Meslin, P.-Y., Forni, O., Royer, C., Mandon, L., et al. (2023). Carbonate Detection With SuperCam in Igneous Rocks on the Floor of Jezero Crater, Mars. *Journal of Geophysical Research: Planets*, *128*(6), e2022JE007463. https://doi.org/10.1029/2022JE007463

Cox, M. A., Cavosie, A. J., Orr, K. J., Daly, L., Martin, L., Lagain, A., et al. (2022). Impact and habitability scenarios for early Mars revisited based on a 4.45-Ga shocked zircon in regolith breccia. *Science Advances*, *8*(5), eabl7497. https://doi.org/10.1126/sciadv.abl7497

Craddock, R. A., & Howard, A. D. (2002). The case for rainfall on a warm, wet early Mars. *Journal of Geophysical Research: Planets*, *107*(E11), 21-1-21–36. https://doi.org/10.1029/2001JE001505

Das, E., & Mitra, K. (2026). Investigating the Formation Conditions of Evaporitic Chloride, Carbonate, and Sulfate Paragenetic Assemblages on Early Mars [Data set]. Zenodo. https://doi.org/10.5281/zenodo.18633200

Das, E., Mitra, K., Hurowitz, J. A., Glotch, T. D., & Bahl, Y. (2026). Paragenetic Formation of Aqueous Alteration Minerals: Thermodynamic Modeling of Basalt Weathering on Early Mars. *Preprint.* ESS Open Archive, 2026(0515). https://doi.org/10.22541/essoar.15003403/v1

Delany, J. M., & Lundeen, S. R. (1991). *LLNL thermochemical data base: Revised data and file format for the EQ3/6 package* (No. DE91017525). Lawrence Livermore National Lab., CA.; Department of Energy, Washington, DC. Retrieved from https://ntrl.ntis.gov/NTRL/dashboard/searchResults/titleDetail/DE91017525.xhtml

Dreibus, G., & Wanke, H. (1985). Mars, a Volatile-Rich Planet. *Meteoritics*, *20*, 367. Retrieved from https://ui.adsabs.harvard.edu/abs/1985Metic..20..367D

Drever, J. I. (1997). *The geochemistry of natural waters: surface and groundwater environments* (3rd ed.). Upper Saddle River, N.J: Prentice Hall.

Ehlmann, B. L., & Edwards, C. S. (2014). Mineralogy of the Martian Surface. *Annual Review of Earth and Planetary Sciences*, *42*(Volume 42, 2014), 291–315. https://doi.org/10.1146/annurev-earth-060313-055024

Ehlmann, B. L., & Mustard, J. F. (2012). An in-situ record of major environmental transitions on early Mars at Northeast Syrtis Major. *Geophysical Research Letters*, *39*(11). https://doi.org/10.1029/2012GL051594

Ehlmann, B. L., Mustard, J. F., Murchie, S. L., Poulet, F., Bishop, J. L., Brown, A. J., et al. (2008). Orbital Identification of Carbonate-Bearing Rocks on Mars. *Science*, *322*(5909), 1828–1832. https://doi.org/10.1126/science.1164759

Ehlmann, B. L., Mustard, J. F., Swayze, G. A., Clark, R. N., Bishop, J. L., Poulet, F., et al. (2009). Identification of hydrated silicate minerals on Mars using MRO-CRISM: Geologic context near Nili Fossae and implications for aqueous alteration. *Journal of Geophysical Research: Planets*, *114*(E2). https://doi.org/10.1029/2009JE003339

El-Maarry, M. R., Pommerol, A., & Thomas, N. (2013). Analysis of polygonal cracking patterns in chloride-bearing terrains on Mars: Indicators of ancient playa settings. *Journal of Geophysical Research: Planets*, *118*(11), 2263–2278. https://doi.org/10.1002/2013JE004463

Elsenousy, A., Hanley, J., & Chevrier, V. F. (2015). Effect of evaporation and freezing on the salt paragenesis and habitability of brines at the Phoenix landing site. *Earth and Planetary Science Letters*, *421*, 39–46. https://doi.org/10.1016/j.epsl.2015.03.047

Eugster, H. P., & Hardie, L. A. (1978). Saline Lakes. In A. Lerman (Ed.), *Lakes: Chemistry, Geology, Physics* (pp. 237–293). New York, NY: Springer. https://doi.org/10.1007/978-1-4757-1152-3_8

Fairén, A. G., Fernández-Remolar, D., Dohm, J. M., Baker, V. R., & Amils, R. (2004). Inhibition of carbonate synthesis in acidic oceans on early Mars. *Nature*, *431*(7007), 423–426. https://doi.org/10.1038/nature02911

Farrand, W. H., Glotch, T. D., Rice, J. W., Hurowitz, J. A., & Swayze, G. A. (2009). Discovery of jarosite within the Mawrth Vallis region of Mars: Implications for the geologic history of the region. *Icarus*, *204*(2), 478–488. https://doi.org/10.1016/j.icarus.2009.07.014

Farrand, W. H., Glotch, T. D., & Horgan, B. (2014). Detection of copiapite in the northern Mawrth Vallis region of Mars: Evidence of acid sulfate alteration. *Icarus*, *241*, 346–357. https://doi.org/10.1016/j.icarus.2014.07.003

Gendrin, A., Mangold, N., Bibring, J.-P., Langevin, Y., Gondet, B., Poulet, F., et al. (2005). Sulfates in Martian Layered Terrains: The OMEGA/Mars Express View. *Science*, *307*(5715), 1587–1591. https://doi.org/10.1126/science.1109087

Gislason, S. R., & Arnórsson, S. (1993). Dissolution of primary basaltic minerals in natural waters: saturation state and kinetics. *Chemical Geology*, *105*(1), 117–135. https://doi.org/10.1016/0009-2541(93)90122-Y

Glotch, T. D., Bandfield, J. L., Tornabene, L. L., Jensen, H. B., & Seelos, F. P. (2010). Distribution and formation of chlorides and phyllosilicates in Terra Sirenum, Mars: CHLORIDES AND

PHYLLOSILICATES ON MARS. *Geophysical Research Letters*, *37*(16). https://doi.org/10.1029/2010GL044557

Glotch, T. D., Bandfield, J. L., Wolff, M. J., Arnold, J. A., & Che, C. (2016). Constraints on the composition and particle size of chloride salt-bearing deposits on Mars: CHLORIDE SALT-BEARING DEPOSITS ON MARS. *Journal of Geophysical Research: Planets*, *121*(3), 454–471. https://doi.org/10.1002/2015JE004921

Halevy, I., & Head III, J. W. (2014). Episodic warming of early Mars by punctuated volcanism. *Nature Geoscience*, *7*(12), 865–868. https://doi.org/10.1038/ngeo2293

Hardie, L. A. (1968). The origin of the Recent non-marine evaporite deposit of Saline Valley, Inyo County, California. *Geochimica et Cosmochimica Acta*, *32*(12), 1279–1301. https://doi.org/10.1016/0016-7037(68)90029-X

Hardie, L. W. A., & Eugster, H. P. (1970). THE EVOLUTION OF CLOSED-BASIN BRINES. *Mineralogical Society of America Special Papers,* 3, 273-290.

Harlov, D. E., & Aranovich, L. (2018). The Role of Halogens in Terrestrial and Extraterrestrial Geochemical Processes: Surface, Crust, and Mantle. In D. E. Harlov & L. Aranovich (Eds.), *The Role of Halogens in Terrestrial and Extraterrestrial Geochemical Processes: Surface, Crust, and Mantle* (pp. 1–19). Cham: Springer International Publishing. https://doi.org/10.1007/978-3-319-61667-4_1

Harvey, R. P., & McSween, H. Y. (1996). A possible high-temperature origin for the carbonates in the martian meteorite ALH84001. *Nature*, *382*(6586), 49–51. https://doi.org/10.1038/382049a0

Harvie, C. E., Møller, N., & Weare, J. H. (1984). The prediction of mineral solubilities in natural waters: The Na-K-Mg-Ca-H-Cl-SO4-OH-HCO3-CO3-CO2-H2O system to high ionic strengths at 25°C. *Geochimica et Cosmochimica Acta*, *48*(4), 723–751. https://doi.org/10.1016/0016-7037(84)90098-X

Hazen, R. M., Downs, R. T., Morrison, S. M., Tutolo, B. M., Blake, D. F., Bristow, T. F., et al. (2023). On the Diversity and Formation Modes of Martian Minerals. *Journal of Geophysical Research: Planets*, *128*(9), e2023JE007865. https://doi.org/10.1029/2023JE007865

Head, J. W., Wilson, L., Dickson, J., & Neukum, G. (2006). The Huygens-Hellas giant dike system on Mars: Implications for Late Noachian–Early Hesperian volcanic resurfacing and climatic evolution. *Geology*, *34*(4), 285. https://doi.org/10.1130/G22163.1

Horgan, B. H. N., Anderson, R. B., Dromart, G., Amador, E. S., & Rice, M. S. (2020). The mineral diversity of Jezero crater: Evidence for possible lacustrine carbonates on Mars. *Icarus*, *339*, 113526. https://doi.org/10.1016/j.icarus.2019.113526

Hurowitz, J. A., Fischer, W. W., Tosca, N. J., & Milliken, R. E. (2010). Origin of acidic surface waters and the evolution of atmospheric chemistry on early Mars. *Nature Geoscience*, *3*(5), 323–326. https://doi.org/10.1038/ngeo831

Hurowitz, J. A., Catling, D. C., & Fischer, W. W. (2023). High Carbonate Alkalinity Lakes on Mars and their Potential Role in an Origin of Life Beyond Earth. *Elements*, *19*(1), 37–44. https://doi.org/10.2138/gselements.19.1.37

Hynek, B. M., Phillips, R. J., & Arvidson, R. E. (2003). Explosive volcanism in the Tharsis region: Global evidence in the Martian geologic record. *Journal of Geophysical Research: Planets*, *108*(E9). https://doi.org/10.1029/2003JE002062

Hynek, B. M., Osterloo, M. K., & Kierein-Young, K. S. (2015). Late-stage formation of Martian chloride salts through ponding and evaporation. *Geology*, *43*(9), 787–790. https://doi.org/10.1130/G36895.1

Irwin, R. P., III, Craddock, R. A., & Howard, A. D. (2005). Interior channels in Martian valley networks: Discharge and runoff production. *Geology*, *33*(6), 489–492. https://doi.org/10.1130/G21333.1

947 Irwin III, R. P., Howard, A. D., Craddock, R. A., & Moore, J. M. (2005). An intense terminal
948 epoch of widespread fluvial activity on early Mars: 2. Increased runoff and paleolake development.
949 *Journal of Geophysical Research: Planets*, *110*(E12). https://doi.org/10.1029/2005JE002460

950 Jiang, C. Z., & Tosca, N. J. (2020). Growth kinetics of siderite at 298.15 K and 1 bar. *Geochimica*
951 *et Cosmochimica Acta*, *274*, 97–117. https://doi.org/10.1016/j.gca.2020.01.047

952 Jones, B. F., & Deocampo, D. M. (2003). 5.13 - Geochemistry of Saline Lakes. In H. D. Holland
953 & K. K. Turekian (Eds.), *Treatise on Geochemistry* (pp. 393–424). Oxford: Pergamon.
954 https://doi.org/10.1016/B0-08-043751-6/05083-0

955 King, P. L., & McLennan, S. M. (2010). Sulfur on Mars. *Elements*, *6*(2), 107–112.
956 https://doi.org/10.2113/gselements.6.2.107

957 Kite, E. S., & Conway, S. (2024). Geological evidence for multiple climate transitions on Early
958 Mars. *Nature Geoscience*, *17*(1), 10–19. https://doi.org/10.1038/s41561-023-01349-2

959 Kite, E. S., Tutolo, B. M., Turner, M. L., Franz, H. B., Burtt, D. G., Bristow, T. F., et al. (2025).
960 Carbonate formation and fluctuating habitability on Mars. *Nature*, *643*(8070), 60–66.
961 https://doi.org/10.1038/s41586-025-09161-1

962 Klingelhöfer, G., Morris, R. V., Bernhardt, B., Schröder, C., Rodionov, D. S., de Souza, P. A., et
963 al. (2004). Jarosite and Hematite at Meridiani Planum from Opportunity's Mössbauer
964 Spectrometer. *Science*, *306*(5702), 1740–1745. https://doi.org/10.1126/science.1104653

965 Langevin, Y., Poulet, F., Bibring, J.-P., & Gondet, B. (2005). Sulfates in the North Polar Region
966 of Mars Detected by OMEGA/Mars Express. *Science*, *307*(5715), 1584.
967 https://doi.org/10.1126/science.1109091

968 Leask, Ellen K., & Ehlmann, B. L. (2022). Evidence for Deposition of Chloride on Mars From
969 Small-Volume Surface Water Events Into the Late Hesperian-Early Amazonian. *AGU Advances*,
970 *3*(1), e2021AV000534. https://doi.org/10.1029/2021AV000534

971 Leask, E. K., Ehlmann, B. L., & Dundar, M. M. (2024). A 2-Billion-Year History of Water-
972 Alteration in Terra Sirenum, Mars: Volcanism's Influence on Aluminum Clay Formation and
973 Chemically Distinct Waters Forming Sulfates and Chlorides Into the Amazonian. *Journal of*
974 *Geophysical Research: Planets*, *129*(10), e2023JE008259. https://doi.org/10.1029/2023JE008259

975 Lowenstein, T. K., & Hardie, L. A. (1985). Criteria for the recognition of salt-pan evaporites.
976 *Sedimentology*, *32*(5), 627–644. https://doi.org/10.1111/j.1365-3091.1985.tb00478.x

977 Marion, Giles M., & Kargel, J. S. (Eds.). (2008). Biogeochemical Applications to Solar System
978 Bodies. In *Cold Aqueous Planetary Geochemistry with FREZCHEM: From Modeling to the*
979 *Search for Life at the Limits* (pp. 101–153). Berlin, Heidelberg: Springer.
980 https://doi.org/10.1007/978-3-540-75679-8_5

981 Marion, Giles M., Kargel, J. S., & Catling, D. C. (2008). Modeling ferrous–ferric iron chemistry
982 with application to martian surface geochemistry. *Geochimica et Cosmochimica Acta*, *72*(1), 242–
983 266. https://doi.org/10.1016/j.gca.2007.10.012

984 Marion, Giles M., Mironenko, M. V., & Roberts, M. W. (2010). FREZCHEM: A geochemical
985 model for cold aqueous solutions. *Computers & Geosciences*, *36*(1), 10–15.
986 https://doi.org/10.1016/j.cageo.2009.06.004

987 Marion, G. M., Kargel, J. S., Crowley, J. K., & Catling, D. C. (2013). Sulfite–sulfide–sulfate–
988 carbonate equilibria with applications to Mars. *Icarus*, *225*(1), 342–351.
989 https://doi.org/10.1016/j.icarus.2013.02.035

990 McCoy, T.J. & Zega T. J. (2025). Composition of asteroid Bennu transformed by aqueous
991 alteration. *Nature Geoscience*, *18*(9), 819–820. https://doi.org/10.1038/s41561-025-01765-6

992 McLennan, S. M. (2022). Chapter 8 - Geochemistry of sedimentary processes on Mars. In J.
993 Filiberto & S. P. Schwenzer (Eds.), *Treatise on Geochemistry (Third Edition): Planetary*
994 *Geochemistry* (pp. 303–339). Elsevier. https://doi.org/10.1016/B978-0-12-813987-5.00008-0

McSween, H. Y., Arvidson, R. E., Bell, J. F., Blaney, D., Cabrol, N. A., Christensen, P. R., et al. (2004). Basaltic Rocks Analyzed by the Spirit Rover in Gusev Crater. *Science*, *305*(5685), 842–845. https://doi.org/10.1126/science.3050842

McSween, H. Y., Ruff, S. W., Morris, R. V., Bell III, J. F., Herkenhoff, K., Gellert, R., et al. (2006a). Alkaline volcanic rocks from the Columbia Hills, Gusev crater, Mars. *Journal of Geophysical Research: Planets*, *111*(E9). https://doi.org/10.1029/2006JE002698

McSween, H. Y., Wyatt, M. B., Gellert, R., Bell III, J. F., Morris, R. V., Herkenhoff, K. E., et al. (2006b). Characterization and petrologic interpretation of olivine-rich basalts at Gusev Crater, Mars. *Journal of Geophysical Research: Planets*, *111*(E2). https://doi.org/10.1029/2005JE002477

McSween, H. Y., Ruff, S. W., Morris, R. V., Gellert, R., Klingelhöfer, G., Christensen, P. R., et al. (2008). Mineralogy of volcanic rocks in Gusev Crater, Mars: Reconciling Mössbauer, Alpha Particle X-Ray Spectrometer, and Miniature Thermal Emission Spectrometer spectra. *Journal of Geophysical Research: Planets*, *113*(E6). https://doi.org/10.1029/2007JE002970

McSween, H. Y., Taylor, G. J., & Wyatt, M. B. (2009). Elemental Composition of the Martian Crust. *Science*, *324*(5928), 736–739. https://doi.org/10.1126/science.1165871

McSween, H. Y., Jr. (2015). Petrology on Mars†. *American Mineralogist*, *100*(11–12), 2380–2395. https://doi.org/10.2138/am-2015-5257

Melwani Daswani, M., & Kite, E. S. (2017). Paleohydrology on Mars constrained by mass balance and mineralogy of pre-Amazonian sodium chloride lakes. *Journal of Geophysical Research: Planets*, *122*(9), 1802–1823. https://doi.org/10.1002/2017JE005319

Meyer C. (2012) Martian Meteorite Compendium — NWA 2737. NASA Johnson Space Center Curation Office, Houston, TX. Available at: https://curator.jsc.nasa.gov/antmet/mmc/nwa2737.pdf

Mitra, K. (2025). Oxychlorine Species on Mars: A Review. *Reviews of Geophysics*, *63*(4), e2024RG000861. https://doi.org/10.1029/2024RG000861

1020 Mitra, K., & Catalano, J. G. (2019). Chlorate as a Potential Oxidant on Mars: Rates and Products
1021 of Dissolved Fe(II) Oxidation. *Journal of Geophysical Research: Planets*, *124*(11), 2893–2916.
1022 https://doi.org/10.1029/2019JE006133

1023 Mitra, K., Catalano, J. G., Bahl, Y., & Hurowitz, J. A. (2023). Iron sulfide weathering by
1024 oxyhalogen species: Implications for iron sulfate and (oxyhydr)oxides formation on Mars. *Earth*
1025 *and Planetary Science Letters*, *624*, 118464. https://doi.org/10.1016/j.epsl.2023.118464

1026 Mitra, K., Malesky, L. A., Thorpe, M. T., & Stevanovic, A. (2025). Siderite and ferric
1027 oxyhydroxides imply interlinked carbon, iron, and halogen cycles on Mars. *Proceedings of the*
1028 *National Academy of Sciences*, *122*(25), e2504674122. https://doi.org/10.1073/pnas.2504674122

1029 Mitra, K., Mitra, S., Gupta, S., Bhattacharya, S., Chauhan, P., & Jain, N. (2018). Modelling basalt
1030 weathering at elevated CO2 concentrations: implications for terminal to post-magmatic rifting in
1031 the Deccan Traps, Kachchh, India. *Geological Society, London, Special Publications*, *463*(1), 227–
1032 241. https://doi.org/10.1144/SP463.8

1033 Mitra, K., Moreland, E. L., & Catalano, J. G. (2020). Capacity of Chlorate to Oxidize Ferrous Iron:
1034 Implications for Iron Oxide Formation on Mars. *Minerals*, *10*(9), 729.
1035 https://doi.org/10.3390/min10090729

1036 Mitra, K., Moreland, E. L., Knight, A. L., & Catalano, J. G. (2022). Rates and Products of Iron
1037 Oxidation by Chlorate at Low Temperatures (0 to 25 °C) and Implications for Mars Geochemistry.
1038 *ACS Earth and Space Chemistry*, *6*(2), 250–260.
1039 https://doi.org/10.1021/acsearthspacechem.1c00379

1040 Mitra, S., Mitra, K., Gupta, S., Bhattacharya, S., Chauhan, P., & Jain, N. (2017). Alteration and
1041 submergence of basalts in Kachchh, Gujarat, India: implications for the role of the Deccan Traps
1042 in the India–Seychelles break-up. *Geological Society, London, Special Publications*, *445*(1), 47–
1043 67. https://doi.org/10.1144/SP445.9

1044 Mojzsis, S. J., & Arrhenius, G. (1998). Phosphates and carbon on Mars: Exobiological
1045 implications and sample return considerations. *Journal of Geophysical Research: Planets*,
1046 *103*(E12), 28495–28511. https://doi.org/10.1029/98JE02141

1047 Morris, R. V., Klingelhöfer, G., Schröder, C., Fleischer, I., Ming, D. W., Yen, A. S., et al. (2008).
1048 Iron mineralogy and aqueous alteration from Husband Hill through Home Plate at Gusev Crater,
1049 Mars: Results from the Mössbauer instrument on the Spirit Mars Exploration Rover. *Journal of*
1050 *Geophysical Research: Planets*, *113*(E12). https://doi.org/10.1029/2008JE003201

1051 Morris, Richard V., Ruff, S. W., Gellert, R., Ming, D. W., Arvidson, R. E., Clark, B. C., et al.
1052 (2010). Identification of Carbonate-Rich Outcrops on Mars by the Spirit Rover. *Science*,
1053 *329*(5990), 421–424. https://doi.org/10.1126/science.1189667

1054 Murchie, S. L., Mustard, J. F., Ehlmann, B. L., Milliken, R. E., Bishop, J. L., McKeown, N. K., et
1055 al. (2009). A synthesis of Martian aqueous mineralogy after 1 Mars year of observations from the
1056 Mars Reconnaissance Orbiter. *Journal of Geophysical Research: Planets*, *114*(E2),
1057 2009JE003342. https://doi.org/10.1029/2009JE003342

1058 Nachon, M., Clegg, S. M., Mangold, N., Schröder, S., Kah, L. C., Dromart, G., et al. (2014).
1059 Calcium sulfate veins characterized by ChemCam/Curiosity at Gale crater, Mars. *Journal of*
1060 *Geophysical Research: Planets*, *119*(9), 1991–2016. https://doi.org/10.1002/2013JE004588

1061 Newsom, H. E., Brittelle, G. E., Hibbitts, C. A., Crossey, L. J., & Kudo, A. M. (1996). Impact
1062 crater lakes on Mars. *Journal of Geophysical Research: Planets*, *101*(E6), 14951–14955.
1063 https://doi.org/10.1029/96JE01139

1064 Niles, P. B., Catling, D. C., Berger, G., Chassefière, E., Ehlmann, B. L., Michalski, J. R., et al.
1065 (2013). Geochemistry of Carbonates on Mars: Implications for Climate History and Nature of
1066 Aqueous Environments. *Space Science Reviews*, *174*(1), 301–328.
1067 https://doi.org/10.1007/s11214-012-9940-y

1068 Ojha, L., Lewis, K., Karunatillake, S., & Schmidt, M. (2018). The Medusae Fossae Formation as
1069 the single largest source of dust on Mars. *Nature Communications*, *9*.
1070 https://doi.org/10.1038/s41467-018-05291-5

1071 Osinski, G. R., Tornabene, L. L., Banerjee, N. R., Cockell, C. S., Flemming, R., Izawa, M. R. M.,
1072 et al. (2013). Impact-generated hydrothermal systems on Earth and Mars. *Icarus*, *224*(2), 347–363.
1073 https://doi.org/10.1016/j.icarus.2012.08.030

1074 Osterloo, M. M., Hamilton, V. E., Bandfield, J. L., Glotch, T. D., Baldridge, A. M., Christensen,
1075 P. R., et al. (2008). Chloride-Bearing Materials in the Southern Highlands of Mars. *Science*,
1076 *319*(5870), 1651–1654. https://doi.org/10.1126/science.1150690

1077 Osterloo, Mikki M., Anderson, F. S., Hamilton, V. E., & Hynek, B. M. (2010). Geologic context
1078 of proposed chloride-bearing materials on Mars. *Journal of Geophysical Research: Planets*,
1079 *115*(E10). https://doi.org/10.1029/2010JE003613

1080 Payré, V., Siebach, K. L., Dasgupta, R., Udry, A., Rampe, E. B., & Morrison, S. M. (2020).
1081 Constraining Ancient Magmatic Evolution on Mars Using Crystal Chemistry of Detrital Igneous
1082 Minerals in the Sedimentary Bradbury Group, Gale Crater, Mars. *Journal of Geophysical*
1083 *Research: Planets*, *125*(8), e2020JE006467. https://doi.org/10.1029/2020JE006467

1084 Peterson, R. C., Nelson, W., Madu, B., & Shurvell, H. F. (2007). Meridianiite: A new mineral
1085 species observed on Earth and predicted to exist on Mars. *American Mineralogist*, *92*(10), 1756–
1086 1759. https://doi.org/10.2138/am.2007.2668

1087 Piercy, J. D., Bridges, J. C., & Hicks, L. J. (2022). Carbonate dissolution and replacement by
1088 odinite and saponite in the Lafayette nakhlite: Part of the CO2-CH4 cycle on Mars? *Geochimica*
1089 *et Cosmochimica Acta*, *326*, 97–118. https://doi.org/10.1016/j.gca.2022.02.003

1090 Pitman, K. M., Dobrea, E. Z. N., Jamieson, C. S., Dalton, J. B., Abbey, W. J., & Joseph, E. C. S.
1091 (2014). What Lurks in the Martian Rocks and Soil? Investigations of Sulfates, Phosphates, and
1092 Perchlorates. Reflectance spectroscopy and optical functions for hydrated Fe-sulfates. *American*
1093 *Mineralogist*, *99*(8–9), 1593–1603. https://doi.org/10.2138/am.2014.4730

1094 Pitzer, K. S. (1973). Thermodynamics of electrolytes. I. Theoretical basis and general equations.
1095 *The Journal of Physical Chemistry*, *77*(2), 268–277. https://doi.org/10.1021/j100621a026

1096 Pitzer, K. S. (Ed.). (1991). *Activity coefficients in electrolyte solutions* (2nd ed). Boca Raton: CRC
1097 Press.

1098 Ramirez, R. M., & Craddock, R. A. (2018). The geological and climatological case for a warmer
1099 and wetter early Mars. *Nature Geoscience*, *11*(4), 230–237. https://doi.org/10.1038/s41561-018-
1100 0093-9

1101 Rampe, E. B., Ming, D. W., Blake, D. F., Bristow, T. F., Chipera, S. J., Grotzinger, J. P., et al.
1102 (2017). Mineralogy of an ancient lacustrine mudstone succession from the Murray formation, Gale
1103 crater, Mars. *Earth and Planetary Science Letters*, *471*, 172–185.
1104 https://doi.org/10.1016/j.epsl.2017.04.021

1105 Rampe, Elizabeth B., Cartwright, J. A., McCubbin, F. M., & Osterloo, M. M. (2018). The Role of
1106 Halogens During Fluid and Magmatic Processes on Mars. In D. E. Harlov & L. Aranovich (Eds.),
1107 *The Role of Halogens in Terrestrial and Extraterrestrial Geochemical Processes* (pp. 959–995).
1108 Cham: Springer International Publishing. https://doi.org/10.1007/978-3-319-61667-4_16

1109 Rampe, E. B., Bristow, T. F., Morris, R. V., Morrison, S. M., Achilles, C. N., Ming, D. W., et al.
1110 (2020). Mineralogy of Vera Rubin Ridge From the Mars Science Laboratory CheMin Instrument.
1111 *Journal of Geophysical Research: Planets*, *125*(9), e2019JE006306.
1112 https://doi.org/10.1029/2019JE006306

1113 Rice, M. S., Bell, J. F., Cloutis, E. A., Wang, A., Ruff, S. W., Craig, M. A., et al. (2010). Silica-
1114 rich deposits and hydrated minerals at Gusev Crater, Mars: Vis-NIR spectral characterization and
1115 regional mapping. *Icarus*, *205*(2), 375–395. https://doi.org/10.1016/j.icarus.2009.03.035

1116 Richardson, J. A., Bleacher, J. E., Connor, C. B., & Glaze, L. S. (2021). Small Volcanic Vents of
1117 the Tharsis Volcanic Province, Mars. *Journal of Geophysical Research: Planets*, *126*(2),
1118 e2020JE006620. https://doi.org/10.1029/2020JE006620

Robbins, S. J., Achille, G. D., & Hynek, B. M. (2011). The volcanic history of Mars: High-resolution crater-based studies of the calderas of 20 volcanoes. *Icarus*, *211*(2), 1179–1203. https://doi.org/10.1016/j.icarus.2010.11.012

Royer, C., Poulet, F., Wiens, R. C., Montmessin, F., Beck, P., Beyssac, O., et al. (2025). The mineralogical composition of Jezero Crater Western Fan: Multigaussian modeling of Perseverance/SuperCam near-infrared observations and overview of major units. *Icarus*, *434*, 116538. https://doi.org/10.1016/j.icarus.2025.116538

Rubin, A., & Ma, C. (2021). *Meteorite Mineralogy*. Cambridge University Press. https://doi.org/10.1017/9781108613767

Ruesch, O., Poulet, F., Vincendon, M., Bibring, J.-P., Carter, J., Erkeling, G., et al. (2012). Compositional investigation of the proposed chloride-bearing materials on Mars using near-infrared orbital data from OMEGA/MEx. *Journal of Geophysical Research: Planets*, *117*(E11). https://doi.org/10.1029/2012JE004108

Scheller, E. L., Ehlmann, B. L., Hu, R., Adams, D. J., & Yung, Y. L. (2021). Long-term drying of Mars by sequestration of ocean-scale volumes of water in the crust. *Science*, *372*(6537), 56–62. https://doi.org/10.1126/science.abc7717

Schwenzer, S. P., Bridges, J. C., Wiens, R. C., Conrad, P. G., Kelley, S. P., Leveille, R., et al. (2016). Fluids during diagenesis and sulfate vein formation in sediments at Gale crater, Mars. *Meteoritics & Planetary Science*, *51*(11), 2175–2202. https://doi.org/10.1111/maps.12668

Sun, V. Z., Hand, K. P., Stack, K. M., Farley, K. A., Simon, J. I., Newman, C., et al. (2023). Overview and Results From the Mars 2020 Perseverance Rover's First Science Campaign on the Jezero Crater Floor. *Journal of Geophysical Research: Planets*, *128*(6), e2022JE007613. https://doi.org/10.1029/2022JE007613

Thomas, N. H., Ehlmann, B. L., Meslin, P.-Y., Rapin, W., Anderson, D. E., Rivera-Hernández, F., et al. (2019). Mars Science Laboratory Observations of Chloride Salts in Gale Crater, Mars. *Geophysical Research Letters*, *46*(19), 10754–10763. https://doi.org/10.1029/2019GL082764

Thorpe, M. T., Bristow, T. F., Rampe, E. B., Tosca, N. J., Grotzinger, J. P., Bennett, K. A., et al. (2022). Mars Science Laboratory CheMin Data From the Glen Torridon Region and the Significance of Lake-Groundwater Interactions in Interpreting Mineralogy and Sedimentary History. *Journal of Geophysical Research: Planets*, *127*(11), e2021JE007099. https://doi.org/10.1029/2021JE007099

Tirsch, D., Bishop, J. L., Voigt, J. R. C., Tornabene, L. L., Erkeling, G., & Jaumann, R. (2018). Geology of central Libya Montes, Mars: Aqueous alteration history from mineralogical and morphological mapping. *Icarus*, *314*, 12–34. https://doi.org/10.1016/j.icarus.2018.05.006

Toner, J. D., Catling, D. C., & Light, B. (2015). Modeling salt precipitation from brines on Mars: Evaporation versus freezing origin for soil salts. *Icarus*, *250*, 451–461. https://doi.org/10.1016/j.icarus.2014.12.013

Tosca, Nicholas J., & McLennan, S. M. (2006). Chemical divides and evaporite assemblages on Mars. *Earth and Planetary Science Letters*, *241*(1), 21–31. https://doi.org/10.1016/j.epsl.2005.10.021

Tosca, N. J., McLennan, S. M., Clark, B. C., Grotzinger, J. P., Hurowitz, J. A., Knoll, A. H., et al. (2005). Geochemical modeling of evaporation processes on Mars: Insight from the sedimentary record at Meridiani Planum. *Earth and Planetary Science Letters*, *240*(1), 122–148. https://doi.org/10.1016/j.epsl.2005.09.042

Tosca, Nicholas J., McLennan, S. M., Lindsley, D. H., & Schoonen, M. A. A. (2004). Acid-sulfate weathering of synthetic Martian basalt: The acid fog model revisited. *Journal of Geophysical Research: Planets*, *109*(E5). https://doi.org/10.1029/2003JE002218

Tosca, Nicholas J., Ahmed, I. A. M., Tutolo, B. M., Ashpitel, A., & Hurowitz, J. A. (2018). Magnetite authigenesis and the warming of early Mars. *Nature Geoscience*, *11*(9), 635–639. https://doi.org/10.1038/s41561-018-0203-8

Trainer, M. G., Wong, M. H., McConnochie, T. H., Franz, H. B., Atreya, S. K., Conrad, P. G., et al. (2019). Seasonal Variations in Atmospheric Composition as Measured in Gale Crater, Mars.

Journal of Geophysical Research: Planets, *124*(11), 3000–3024. https://doi.org/10.1029/2019JE006175

Treiman, A. H., Bish, D. L., Vaniman, D. T., Chipera, S. J., Blake, D. F., Ming, D. W., et al. (2016). Mineralogy, provenance, and diagenesis of a potassic basaltic sandstone on Mars: CheMin X-ray diffraction of the Windjana sample (Kimberley area, Gale Crater). *Journal of Geophysical Research: Planets*, *121*(1), 75–106. https://doi.org/10.1002/2015JE004932

Tutolo, B. M., Hausrath, E. M., Kite, E. S., Rampe, E. B., Bristow, T. F., Downs, R. T., et al. (2025). Carbonates identified by the Curiosity rover indicate a carbon cycle operated on ancient Mars. *Science*, *388*(6744), 292–297. https://doi.org/10.1126/science.ado9966

Vaniman, David T., Bish, D. L., Chipera, S. J., Fialips, C. I., William Carey, J., & Feldman, W. C. (2004). Magnesium sulphate salts and the history of water on Mars. *Nature*, *431*(7009), 663–665. https://doi.org/10.1038/nature02973

Vaniman, D. T., Bish, D. L., Ming, D. W., Bristow, T. F., Morris, R. V., Blake, D. F., et al. (2014). Mineralogy of a Mudstone at Yellowknife Bay, Gale Crater, Mars. *Science*, *343*(6169), 1243480. https://doi.org/10.1126/science.1243480

Vaniman, David T., Martínez, G. M., Rampe, E. B., Bristow, T. F., Blake, D. F., Yen, A. S., et al. (2018). Gypsum, bassanite, and anhydrite at Gale crater, Mars. *American Mineralogist*, *103*(7), 1011–1020. https://doi.org/10.2138/am-2018-6346

Wang, A., Freeman, J. J., Chou, I.-M., & Jolliff, B. L. (2011). Stability of Mg-sulfates at −10°C and the rates of dehydration/rehydration processes under conditions relevant to Mars. *Journal of Geophysical Research: Planets*, *116*(E12). https://doi.org/10.1029/2011JE003818

Wang, A., Freeman, J. J., & Jolliff, B. L. (2009). Phase transition pathways of the hydrates of magnesium sulfate in the temperature range 50°C to 5°C: Implication for sulfates on Mars. *Journal of Geophysical Research: Planets*, *114*(E4). https://doi.org/10.1029/2008JE003266

1195 Wang, A., Haskin, L. A., Squyres, S. W., Jolliff, B. L., Crumpler, L., Gellert, R., et al. (2006).
1196 Sulfate deposition in subsurface regolith in Gusev crater, Mars. *Journal of Geophysical Research:*
1197 *Planets*, *111*(E2). https://doi.org/10.1029/2005JE002513

1198 Whelley, P., Matiella Novak, A., Richardson, J., Bleacher, J., Mach, K., & Smith, R. N. (2021).
1199 Stratigraphic Evidence for Early Martian Explosive Volcanism in Arabia Terra. *Geophysical*
1200 *Research Letters*, *48*(15), e2021GL094109. https://doi.org/10.1029/2021GL094109

1201 Wordsworth, R. D. (2016). The Climate of Early Mars. *Annual Review of Earth and Planetary*
1202 *Sciences*, *44*(Volume 44, 2016), 381–408. https://doi.org/10.1146/annurev-earth-060115-012355

1203 Wordsworth, R., Knoll, A. H., Hurowitz, J., Baum, M., Ehlmann, B. L., Head, J. W., & Steakley,
1204 K. (2021). A coupled model of episodic warming, oxidation and geochemical transitions on early
1205 Mars. *Nature Geoscience*, *14*(3), 127–132. https://doi.org/10.1038/s41561-021-00701-8

1206 Wray, James J., Murchie, S. L., Bishop, J. L., Ehlmann, B. L., Milliken, R. E., Wilhelm, M. B., et
1207 al. (2016). Orbital evidence for more widespread carbonate-bearing rocks on Mars. *Journal of*
1208 *Geophysical Research: Planets*, *121*(4), 652–677. https://doi.org/10.1002/2015JE004972

1209 Wray, J. J., Noe Dobrea, E. Z., Arvidson, R. E., Wiseman, S. M., Squyres, S. W., McEwen, A. S.,
1210 et al. (2009). Phyllosilicates and sulfates at Endeavour Crater, Meridiani Planum, Mars.
1211 *Geophysical Research Letters*, *36*(21). https://doi.org/10.1029/2009GL040734

1212 Ye, C., & Glotch, T. D. (2019). Spectral Properties of Chloride Salt-Bearing Assemblages:
1213 Implications for Detection Limits of Minor Phases in Chloride-Bearing Deposits on Mars. *Journal*
1214 *of Geophysical Research: Planets*, *124*(2), 209–222. https://doi.org/10.1029/2018JE005859

1215 Zastrow, A. M., & Glotch, T. D. (2021). Distinct Carbonate Lithologies in Jezero Crater, Mars.
1216 *Geophysical Research Letters*, *48*(9). https://doi.org/10.1029/2020GL092365

1217 Zolotov, M. Y., & Mironenko, M. V. (2007). Timing of acid weathering on Mars: A kinetic-
1218 thermodynamic assessment. Journal of Geophysical Research: Planets, 112(E7).
1219 https://doi.org/10.1029/2006JE002882

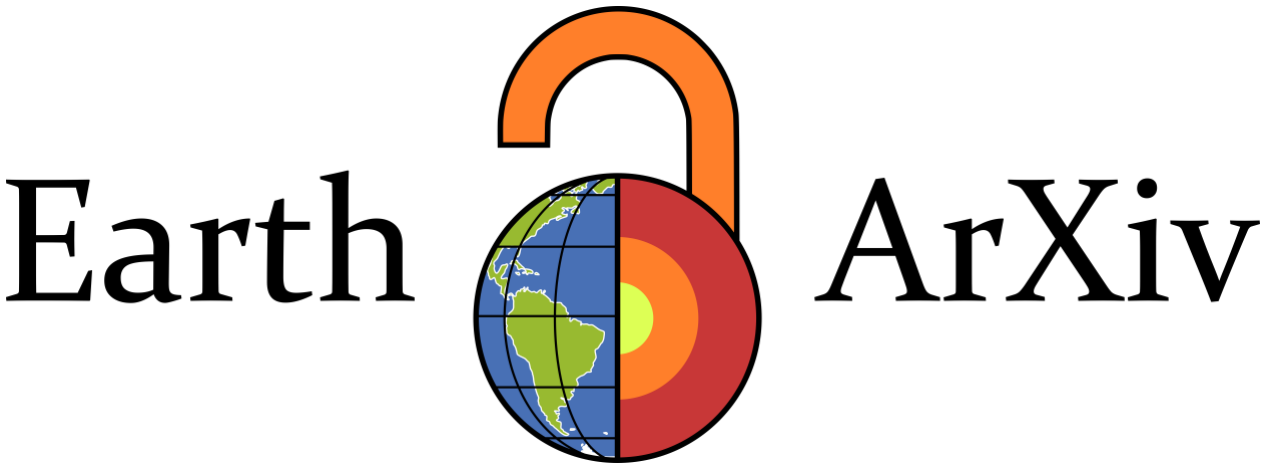

Supporting Information for:

Investigating the Formation Conditions of Evaporitic Chloride, Carbonate, and Sulfate Paragenetic Assemblages on Early Mars

Eashan Das[1], Kaushik Mitra[1,2,3†], Joel A. Hurowitz[1], Timothy D. Glotch[1], and Yatharth Bahl[1]

[1]Department of Geosciences, Stony Brook University, Stony Brook, NY 11794 USA.

[2]Department of Earth & Planetary Sciences, The University of Texas at San Antonio, San Antonio, TX 78249 USA

[3]Department of Physics & Astronomy, The University of Texas at San Antonio, San Antonio, TX 78249 USA.

†Corresponding author:

Kaushik Mitra (kaushik.mitra@utsa.edu)

Supplementary Information for

Investigating the Formation Conditions of Evaporitic Chloride, Carbonate, and Sulfate Paragenetic Assemblages on Early Mars

Eashan Das[1], Kaushik Mitra[1,2,3]†, Joel A. Hurowitz[1], Timothy D. Glotch[1], and Yatharth Bahl[1]

[1]Department of Geosciences, Stony Brook University, Stony Brook, NY 11794 USA.

[2]Department of Earth & Planetary Sciences, The University of Texas at San Antonio, San Antonio, TX 78249 USA

[3]Department of Physics & Astronomy, The University of Texas at San Antonio, San Antonio, TX 78249 USA.

†Corresponding author:

Kaushik Mitra (kaushik.mitra@utsa.edu)

Contents of this file

Introduction

Included here are Sections S1-2 including descriptions of suppressed phases, and k-means clustering. Table S1 containing substrate composition. Figures S1-S5 which show leachate compositions.

Section S1: Suppressed Phases

We suppressed the formation of the listed minerals as their formation in the pressure-temperature conditions relevant to the surface of Mars is kinetically unfavorable. Additionally, organic species were suppressed as conversion of dissolved C(IV) to organic speciies is unlikely on Mars to ensure that C(IV) reactions were between inorganic species only.

The minerals suppressed were: Albite, Albite_high, Albite_low, Amesite, Amesite-14A, Andradite, Annite, Antigorite, Berthierine, Boehmite-llnl, Boehmite-Nordstrom, Celadonite, Chlorapatite, Chromite, Clinochlore-14A, Clinochlore-7A, Daphnite-14A, Daphnite-7A, Diaspore, Diopside, Dolomite, Dolomite-dis, Dolomite-ord, En38Fs62_Pyroxene, Enstatite, Epidote, Epidote-ord, Foshagite, Hedenbergite, Hematite, Ilmenite, Maximum_Microcline, Mesolite, Minnesotaite, Monticellite, Muscovite, Natrolite, Nepheline, Okenite, Paragonite, Phlogopite, Pimelate, Quartz, Rankinite, Rutile, Sanidine_high, Scolecite, Sebacate, Stilbite, Suberate, Succinate, Tobermorite-11A, Tobermorite-14A, Tobermorite-9A, Tremolite, Tridymite, Troilite, Wollastonite, Xonotlite,

Section S2: K-Means Clustering

We applied the K-means statistical clustering algorithm to a dataset consisting of the final leached quantities of major mineral forming ions (Mg^{2+}, Fe^{2+}, Na^{+}, Ca^{2+}, Cl^{-}, HCO_3^{-}, SO_4^{2-}) dissolved in the formed leachates for each iteration. The input quantities were transformed using a base-10 logarithm to reduce the dynamic range and mitigate the influence of highly skewed concentrations. Clustering was then performed on this dataset using MATLAB's built-in *kmeans* function. To improve the robustness and avoid local minima we ran the algorithm using 20 replicates, and retained the best solution based on the total within-cluster sum of squares. For interpretability, the original (non-log transformed) concentrations of ions were averaged within each cluster to characterize the mean composition of each identified leachate type (cluster center). The algorithm labeled each input leachate with an assigned leachate type depending on the choice of the number of clusters (k).

We implemented an iterative approach for determining the number of clusters (k). We began with k = 2 and incrementally increased to k = 7, evaluating if each cluster solution was a chemically meaningful grouping that was observable in the original leachate composition data. To do so, after each iteration, the assigned cluster labels (i.e., leachate types) were overlaid on original compositional plots to visually inspect whether the clusters identified corresponded to chemically meaningful groupings. Ultimately, we integrated insights from our k-means clustering outputs, ternary diagram compositional patterns (Figs. S1-S2), and leachate compositions (Figs. S3-S4) and identified 8 distinct leachate types.

89

Mineral Phase	**Mineral Weight (g)**	**Weight %**
Quartz	1.00E-05	1.01E-05
Albite	22.45	22.70
Anorthite	17.39	17.58
Diopside	16.43	16.61
Forsterite	13.05	13.19
Magnetite	3.1	3.13
Fayalite	15.93	16.10
Enstatite	3.76	3.80
Ferrosilite	3.76	3.80
K-Feldspar	0.66	0.67
Chromite	0.88	0.89
Chlorapatite	1.51	1.53
Total	**98.92**	**100.00**

90 **Table S1:** Composition of substrate, Mazatzal basalt, used in our modeling study.
91

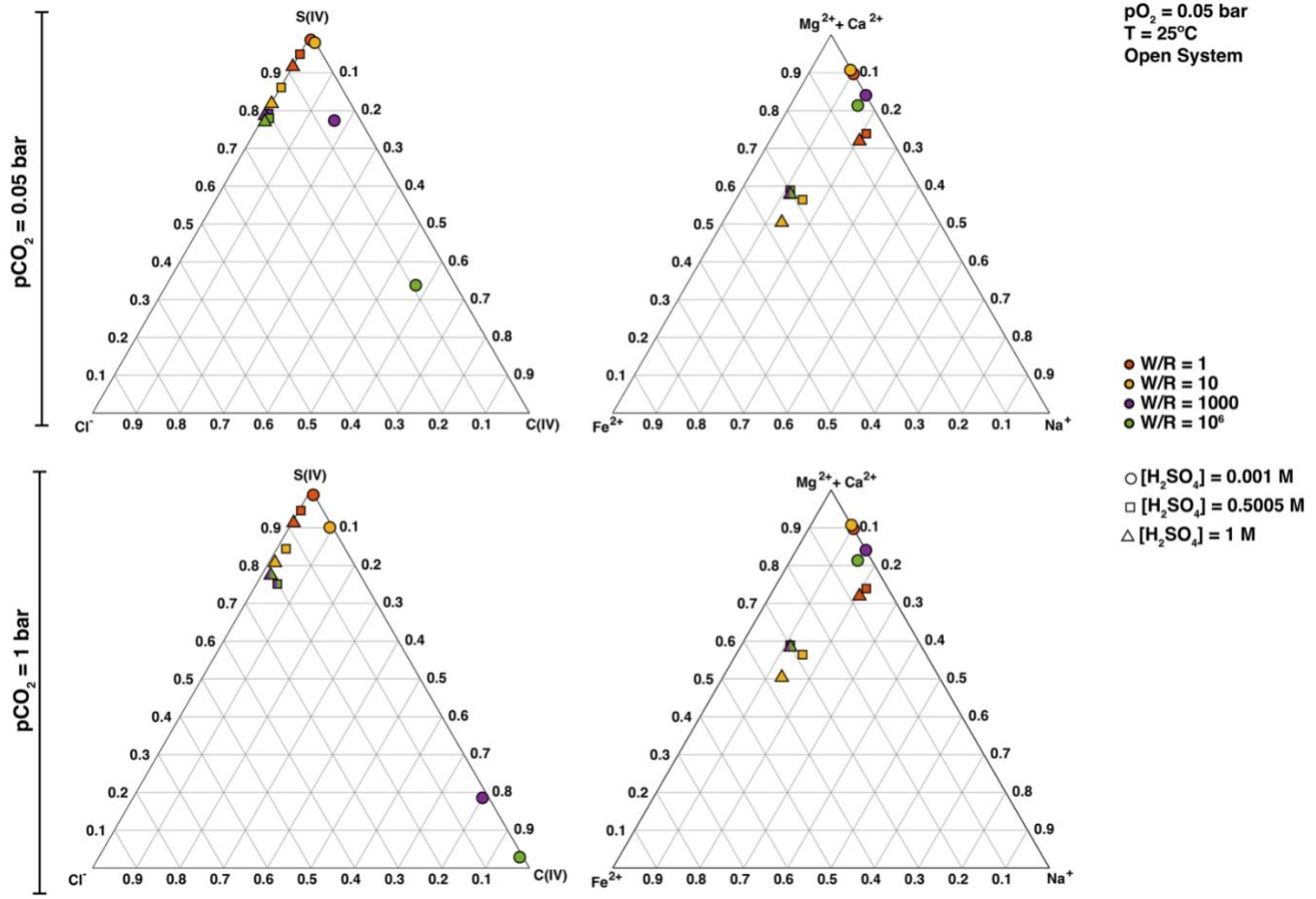

Figure S1: *Open System leachate compositions plotted on ternary diagrams. Top left are leachate plotted on the $Cl^-/HCO_3^-/SO_4^{2-}$ ternary at pCO2 = 0.05 bar, top right shows cation compositions plotted on the $Fe^{2+}/(Mg^{2+} + Ca^{2+})/Na^+$ ternary at pCO_2 = 0.05 bar, bottom left are leachates plotted on the $Cl^-/HCO_3^-/SO_4^{2-}$ ternary at pCO_2 = 1 bar bottom right shows cation compositions plotted on the $Fe^{2+}/(Mg^{2+} + Ca^{2+})/Na^+$ ternary at pCO_2 = 1 bar.*

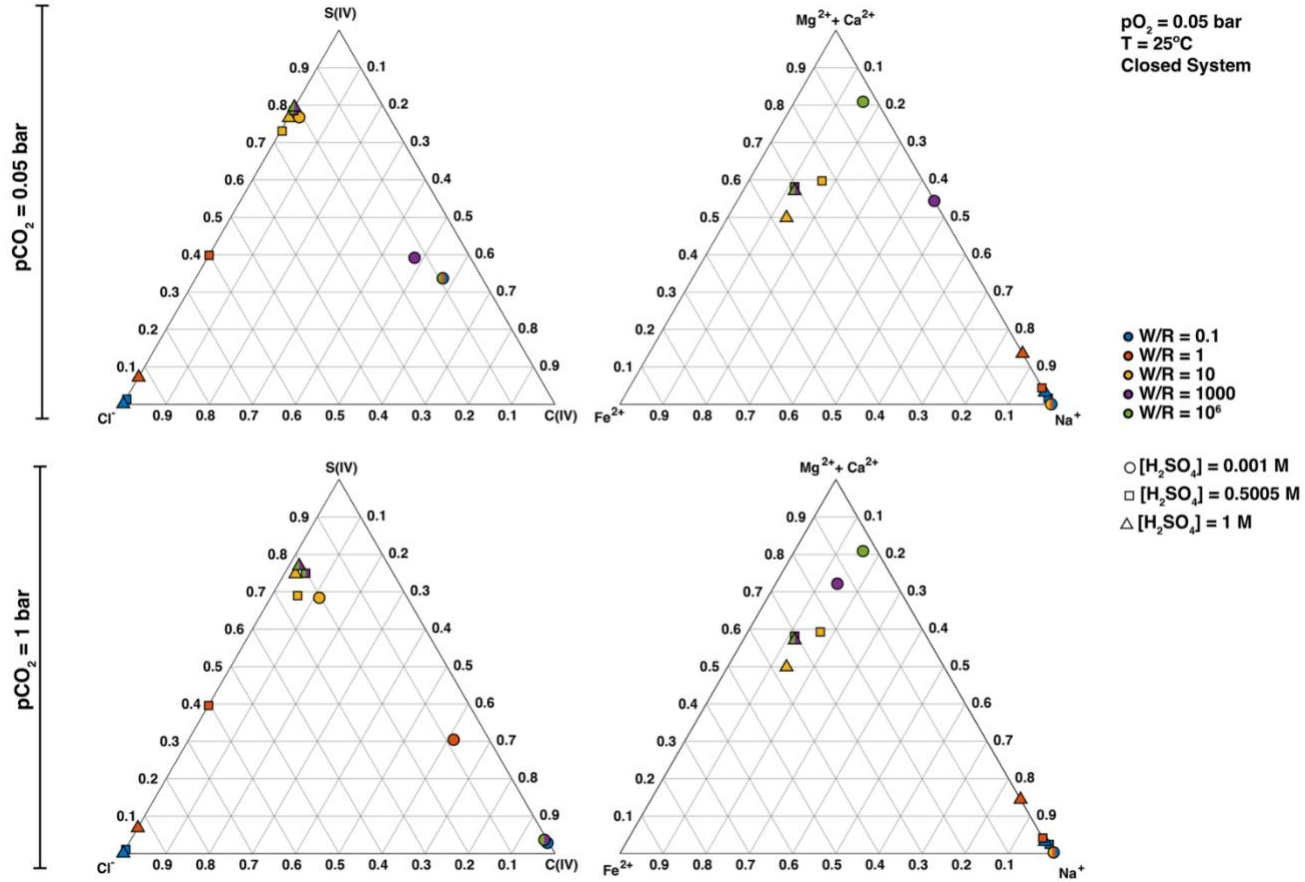

Figure S2: *Closed system leachates compositions plotted on ternary diagrams. Top left are leachates plotted on the $Cl^-/HCO_3^-/SO_4^{2-}$ ternary at pCO_2 = 0.05 bar, top right shows cation compositions plotted on the $Fe^{2+}/(Mg^{2+} + Ca^{2+})/Na^+$ ternary at pCO_2 = 0.05 bar, bottom left are leachates plotted on the $Cl^-/HCO_3^-/SO_4^{2-}$ ternary at pCO_2 = 1 bar, bottom right shows cation compositions plotted on the $Fe^{2+}/(Mg^{2+} + Ca^{2+})/Na^+$ ternary at pCO_2 = 1 bar. All leachates are comparatively shifted towards the Cl^- apex compared to the open system, however, a majority of leachates do fall near the SO_4^{2-} apex. Moderate-high initial acidity and low W/R create leachates that are Na and Cl rich. Low/moderate W/R leachates are Na rich while higher W/R favors a more Mg^{2+}/Ca^{2+} rich leachate.*

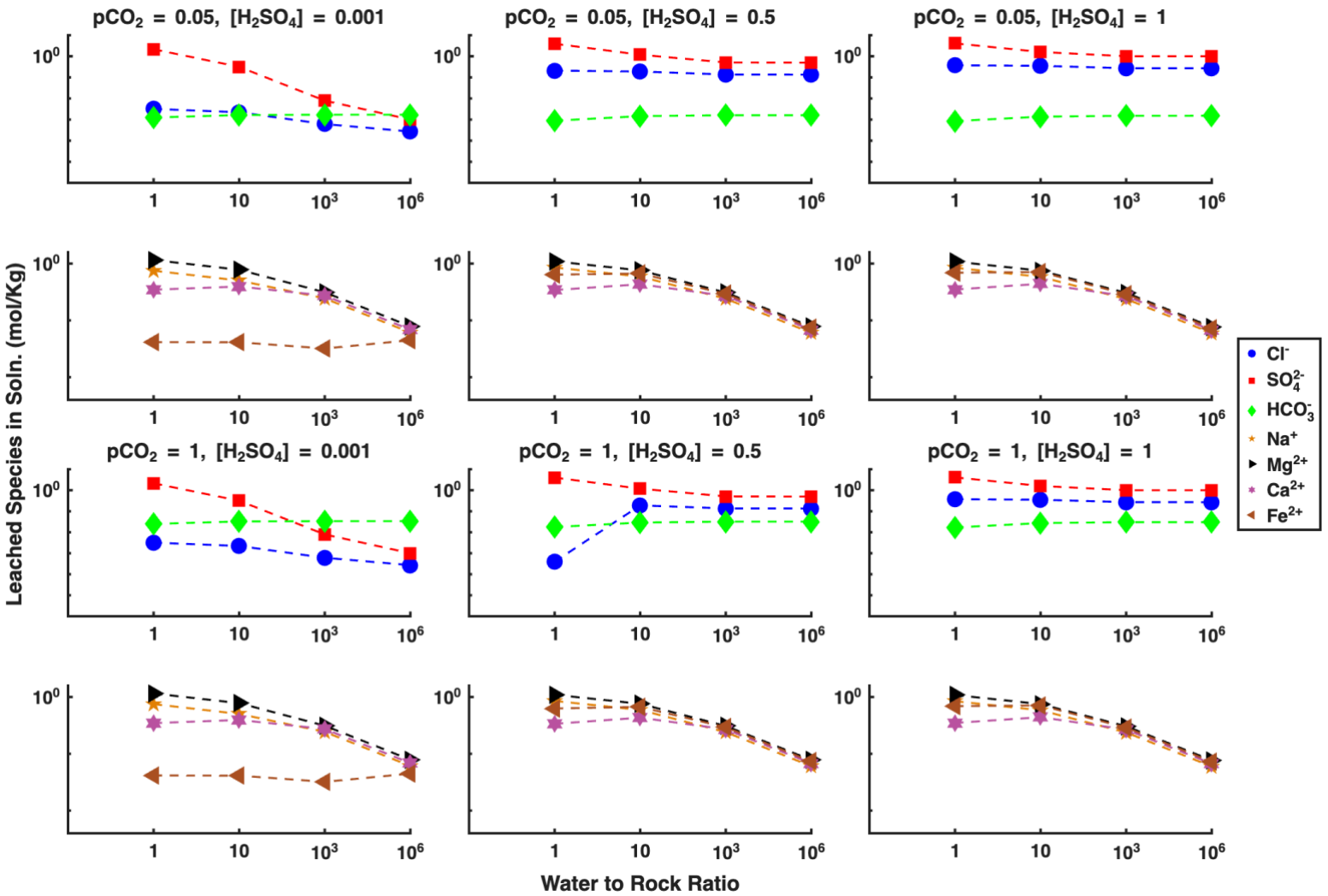

Figure S3: *Concentrations of major species in leachate solutions (in mol/Kg) generated from our open system models. Here we show quantities of major evaporite mineral forming anions in the leachate (Cl^-, C(IV), S(VI)) and cations (Na^+, Mg^{2+}, Fe^{2+}, Ca^{2+}) as Water-to-Rock ratio (W/R) is varied from 0.1 to 10^6.*

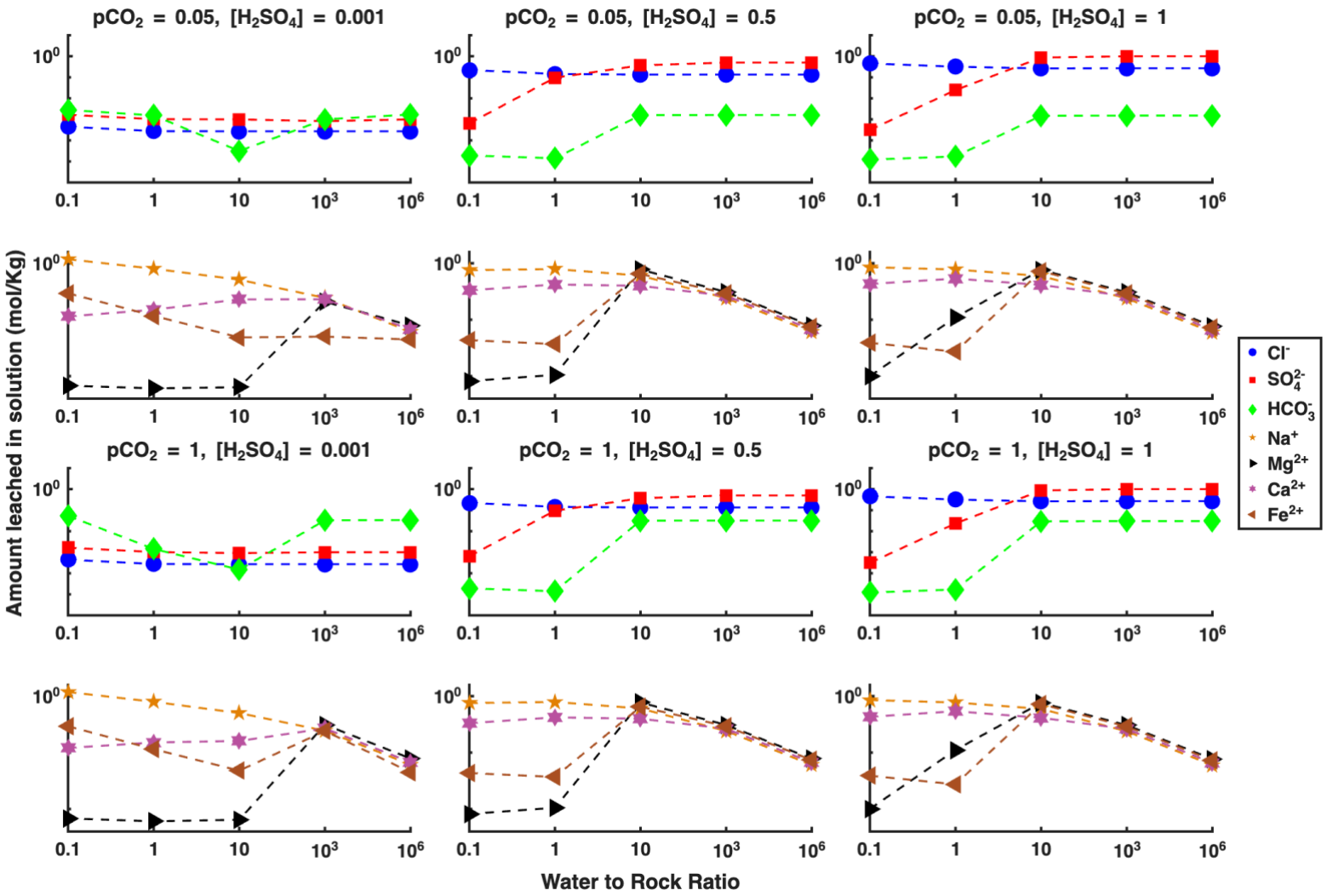

Figure S4: *Concentrations of major species in leachate solutions (in mol/Kg) generated from our closed system models. Here we show quantities of major evaporite mineral forming anions in the leachate (Cl^-, C(IV), S(VI)) and cations (Na^+, Mg^{2+}, Fe^{2+}, Ca^{2+}) as Water-to-Rock ratio (W/R) is varied from 0.1 to 10^6.*

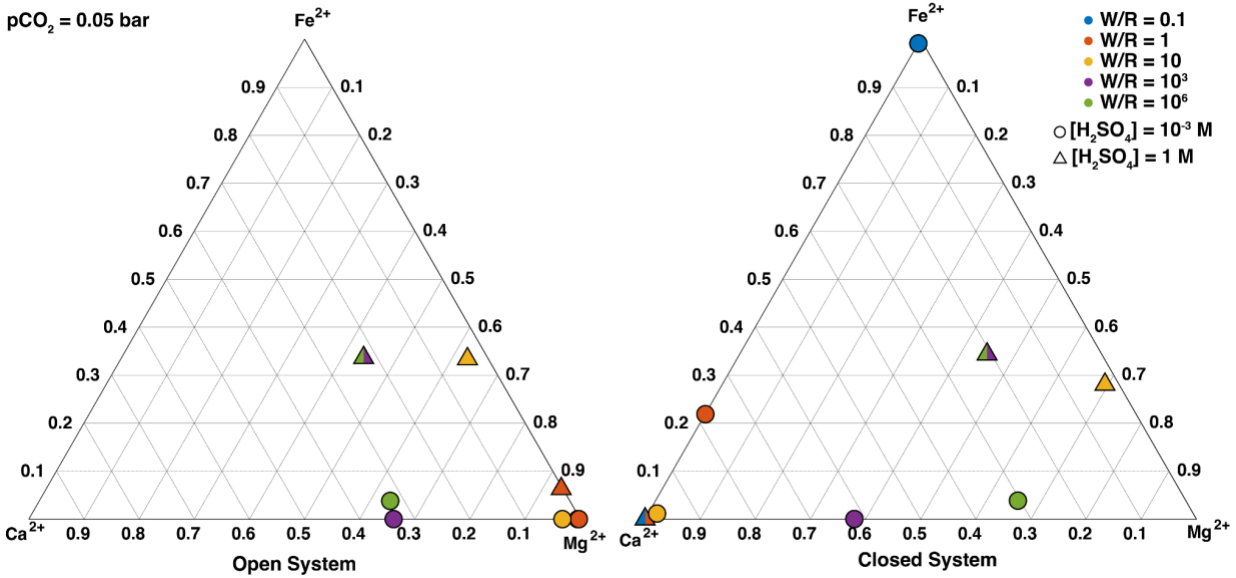

Figure S5: *Composition of leachates on a $Ca^{2+}/Mg^{2+}/Fe^{2+}$ ternary diagram for open (left) and closed (right) system weathering. Compositions are shown for a subset of models where pCO_2 = 0.05 bar. Open system leachates are Mg^{2+} rich, while closed system leachates show greater variability. Low W/R closed system leachates tend to be Ca^{2+} dominated, while increasing W/R and initial H_2SO_4 leads to Mg^{2+} dominated leachates similar to open system weathering. Circle markers are used to indicate $[H_2SO_4]$ = 0.001 M, while triangle markers indicate $[H_2SO_4]$ = 1 M. Markers with split colors indicate the composition on the ternary is the same for more than one W/R*

120